Electron Boltzmann equation in nonthermal plasmas

J. A. Kunc and W. H. Soon
Departments of Aerospace Engineering and Physics, University of Southern California, Los Angeles, Caliornia 90089-1191
(Received 29 June 1990)

Numerical and analytical solutions of the electron Boltzmann equation in two-temperature steady-state helium plasma are studied in a broad range of conditions (5000 K $\leq T_a \leq$ 20 000 K, 10 000 K $\leq T_e \leq$ 20 000 K; 10^{10} cm$^{-3} \leq N_a \leq 10^{18}$ cm^{-3}). The WKB analytical solution is found to be satisfactory in most situations. The deviation of the electron distribution from Maxwellian and a possibility of raising of the tail of the distribution is also discussed.

INTRODUCTION

It is well known[1-4] that deviation of the electron energy distribution from the Maxwellian distribution can be significant in weakly ionized gases where one, or more, of the lowest excited levels of neutral species are strongly radiative and where the radiation produced by these levels is poorly reabsorbed in the gas. Then, the energy lost by fast electrons to excite the levels cannot be regained by electrons and the number of the fast electrons in the plasma is greatly reduced. (Since in such a case the electron distribution differs from Maxwellian distribution only at energies $\varepsilon \gg kT_e$, one can still use the concept of temperature.)

The first two excited levels in helium atoms are metastable, and the populations of these levels can be relatively large in some situations (see below). Consequently, the following atom-impact processes in helium can directly produce fast electrons, overpopulating the tail of the electron distribution; the Penning ionization:

$$\mathrm{He}(2\,^3S_1)+\mathrm{He}(2\,^3S_1)\rightarrow e(\varepsilon)+\mathrm{He}(1\,^1S_0)+\mathrm{He}^+(1\,^2S_{1/2})\ , \tag{1}$$

the associative ionization:

$$\mathrm{He}(2\,^3S_1)+\mathrm{He}(2\,^3S_1)\rightarrow e(\varepsilon)+\mathrm{He}_2^+(X\,^2\Sigma_u^+,v)\ , \tag{2}$$

and the electron-impact deexcitation of the $\mathrm{He}(2\,^3S_1)$ atoms:

$$e(\varepsilon-\varepsilon_{12})+\mathrm{He}(2\,^3S_1)\rightarrow e(\varepsilon)+\mathrm{He}(1\,^1S_0)\ , \tag{3}$$

where ε is the electron energy and ε_{12} is the energy gap between the ground state and the first excited level of the helium atom. It is obvious then, that a possibility of raising the tail of the electron distribution above the Maxwellian tail is quite realistic in helium plasmas with a large number of metastable atoms.[5-8] Such situations occur, for example, in some afterglow plasmas where the number of metastable atoms produced during the transient phase of the discharge can be quite large. In general, the populations and the energy (translational and internal) distributions of particles in the beginning of the steady-state phase (following the transient phase) depend on the way in which energy is supplied to the gas in the transient phase. The relaxation time for electron energy is usually much shorter than the relaxation times for the energies (internal and translational) of atomic species. Therefore a stationary electron distribution can be established (after the end of the transient phase) and be maintained for a meaningful period of time during which parameters T_e, T_a N_e, N_1, and N_2 remain constant. Consequently, the ratios $H_{n_{\max}}=N_e/N_e^S$ and $B_2=N_2/N_2^B$ [N_e^S and N_2^B are populations of electrons and the metastable $\mathrm{He}(2\,^3S_1)$ atoms, respectively, in local thermal equilibrium (LTE)] in the beginning of the steady state can differ from case to case by orders of magnitude. We study in this work the properties of the stationary Boltzmann equation for electrons as a function of T_e, T_a, N_a (T_a and N_a are atomic temperature and density, respectively), $H_{n_{\max}}$, and B_2 existing at the end of the transient phase (i.e., at the beginning of the steady-state phase).

The three-level electronic energy structure (the ground state, the first excited state, and continuum) assumed for helium is numbered sequentially, with $i=1$ for the ground state, $i=2$ for the first excited level, and c for continuum (the ground-state ion). The positive ions are considered to be singly ionized and in the ground states. Such energy structure is a sufficient representation of the atomic properties for acceptable predictions of the main features of the electron distribution in the plasmas considered in this work (see Ref. 6 and discussion below).

The following processes, important for direct and indirect population of the fast electrons in the plasma, are taken into account in addition to the processes (1)–(3): the electron-impact excitation and deexcitation:

$$e(\varepsilon)+\mathrm{He}(1\,^1S_0)\rightleftarrows e(\varepsilon+\varepsilon_{12})+\mathrm{He}(2\,^3S_1)\ , \tag{4}$$

the electron-impact ionization and three-body recombination:

$$e(\varepsilon)+\mathrm{He}(1\,^1S_1)\rightleftarrows e(\varepsilon')+e(\varepsilon_b)+\mathrm{He}^+(1\,^2S_{1/2})\ , \tag{5}$$

the electron-impact ionization and three-body recombination:

$$e(\varepsilon)+\mathrm{He}(2\,^3S_1)\rightleftarrows e(\varepsilon')+e(\varepsilon_b)+\mathrm{He}^+(1\,^2S_{1/2})\ , \tag{6}$$

the radiative recombination producing $\mathrm{He}(1\,^1S_0)$ atoms:

$$e(\varepsilon)+\mathrm{He}^+(1\,^2S_{1/2})\rightarrow\mathrm{He}(1\,^1S_0)+h\nu\ , \tag{7}$$

the radiative recombination producing $\mathrm{He}(2\,^3S_1)$ atoms:

$$e(\varepsilon)+\mathrm{He}^+(1\,^2S_{1/2})\rightarrow\mathrm{He}(2\,^3S_1)+h\nu\ , \tag{8}$$

the atom-impact ionization of $\mathrm{He}(1\,^1S_0)$ atoms:

$$\mathrm{He}(1\,^1S_0)+\mathrm{He}(1\,^1S_0)\rightarrow\mathrm{He}(1\,^1S_0)+\mathrm{He}(1\,^2S_{1/2})+e(\varepsilon)\ , \tag{9}$$

and the atom-impact ionization of $\mathrm{He}(2\,^3S_1)$ atoms:

$$\mathrm{He}(1\,^1S_0)+\mathrm{He}(2\,^3S_1)\rightarrow\mathrm{He}(1\,^1S_0)+\mathrm{He}^+(1\,^2S_{1/2})+e(\varepsilon)\ , \tag{10}$$

where conservation of energy requires that in the processes (5) and (6)

$$\varepsilon=U_i+\varepsilon'+\varepsilon_b\ , \tag{11}$$

and the processes (7) and (8)

$$h\nu=\varepsilon+U_i\ . \tag{12}$$

Here, U_i is the ionization potential for the ith atomic level, ε' is the energy of the incident electron after collision, and ε_b is the energy of the ejected electron. Since we consider both electron-atom and atom-atom inelastic collisions, we use a two-temperature model in which the electron temperature T_e can differ from the atomic temperature T_a; the energy distribution of atoms is assumed to be a Maxwellian distribution.

The electron energy distribution is obtained from the stationary Boltzmann equation,

$$\mathbf{v}\cdot\frac{\partial}{\partial\mathbf{r}}(N_e f)+\frac{\mathbf{F}}{m_e}\cdot\frac{\partial}{\partial\mathbf{v}}(N_e f)=\left[\frac{\delta}{\delta t}(N_e f)\right]_{\mathrm{coll}}\ , \tag{13}$$

where $\mathbf{v}$ is the electron velocity, $\mathbf{r}$ is the spatial coordinate, $\mathbf{F}/m_e$ is the external force (per unit mass) acting on the electron, and the term on the right-hand side is the collision term. We consider below physical conditions for which the left-hand side of Eq. (13) is small compared with the collision terms on the right-hand side. Then, Eq. (13) becomes

$$\left[\frac{\delta(N_e f)}{\delta t}\right]_{\mathrm{coll}}=\left[\frac{\delta(N_e f)}{\delta t}\right]_{\mathrm{el}}+\left[\frac{\delta(N_e f)}{\delta t}\right]_{\mathrm{in}}=0\ , \tag{14}$$

where the subscripts el and in relate to elastic and inelastic collisions, respectively, and the distribution f is isotropic in the phase space and depends only parametrically on position. The normalization condition for the electron distribution is

$$\int_0^\infty \varepsilon^{1/2} f(\varepsilon)d\varepsilon=1\ , \tag{15}$$

so that the Maxwellian distribution is given by

$$f^*(\varepsilon)=\frac{2}{\sqrt{\pi}}\frac{1}{(kT_e)^{3/2}}e^{-\varepsilon/kT_e} \tag{16}$$

(the asterisk denotes the thermal equilibrium) and the rate coefficient for an electron-impact binary collision is

$$C=\left[\frac{2}{m_e}\right]^{1/2}\int_0^\infty Q(\varepsilon)\varepsilon f(\varepsilon)d\varepsilon\ , \tag{17}$$

where $Q(\varepsilon)$ is the cross section for the process.

COLLISION TERMS

The collision terms of Eq. (14) multiplied by $4\pi v^2 dv=4\pi(2\varepsilon)^{1/2}m_e^{-3/2}d\varepsilon$ give the rates per unit volume at which electrons enter the energy range $[\varepsilon,\varepsilon+d\varepsilon]$ as a result of elastic or inelastic collisions. The terms are derived below using the formulations of Shkarofsky, Johnston, and Bachynski,[9] Viegas,[10] Mitchner and Kruger,[11] and Shoub.[3]

Electron-electron collisions

The common electron-electron collision term is based, at all energies, on the Fokker-Planck formalism.[9] However, it was shown by Peyraud[12–14] that in plasmas with very high density of metastable atoms, this representation can be inaccurate for description of the high-energy tail of the electron distribution. It was suggested that in such plasmas the Balescu-Lenard formalism[15] should be used in the high-energy range. The difficulty can be seen in the behavior of the function $C(\varepsilon)$ [Eq. (57)], particularly through the term with $f(\varepsilon-\varepsilon_{12})$. This term represents the contribution of fast electrons produced by process (3) and it dominates the other terms in Eq. (57) at energies $\varepsilon\gtrsim\varepsilon_{12}$ if the relative population of the metastable atoms is very large. As a result, unrealistic periodic "humps" occur on the tail of the distribution at $\varepsilon\approx n\varepsilon_{12}$ (where $n\geq 2$). If the Balescu-Lenard collision term is used in the Boltzmann equation these "humps" are smeared out.[12]

To avoid the difficulties associated with the complexity of the Balescu-Lenard formalism, we use the Fokker-Planck collision term in all situations, including the high-energy region in plasmas with very large population of the metastable atoms. Then, the high-energy tail of the electron distribution can be taken, in the first-order approximation, as $f^*(\varepsilon-\varepsilon_{12})$. A numerical analysis shows that such a procedure is appropriate to obtain reasonable estimates of the rate coefficients even for electron-impact ionization of the ground state in plasmas with relatively large population of the metastable atoms. This is because in such a case the production of electrons is dominated not by the ground-state ionization, but by processes (1) and (2) that involve metastable atoms and which are controlled by the medium-energy part of the electron distribution (see discussion below).

The Fokker-Planck collision term for the electron-electron scattering is

$$\left[\frac{\delta f}{\delta t}\right]_{e\text{-}e}=N_e(2\varepsilon/m_e)^{1/2}\frac{1}{\varepsilon}\frac{d}{d\varepsilon}\times\left[a_e(\varepsilon)\frac{df(\varepsilon)}{d\varepsilon}+b_e(\varepsilon)f(\varepsilon)\right]\ , \tag{18}$$

where

$$a_e(\varepsilon)=2(kT_e)^2\bar{Q}_{e\text{-}e}\left[\int_0^{\varepsilon}\varepsilon^{3/2}f(\varepsilon)d\varepsilon+\varepsilon^{3/2}\int_{\varepsilon}^{\infty}f(\varepsilon)d\varepsilon\right], \tag{19}$$

$$b_e(\varepsilon)=3(kT_e)^2\bar{Q}_{e\text{-}e}\int_0^{\varepsilon}\varepsilon^{1/2}f(\varepsilon)d\varepsilon, \tag{20}$$

$$\bar{Q}_{e\text{-}e}=6\pi(e^2/3kT_e)^2\ln\Lambda, \tag{21}$$

and where k and e are Boltzmann's constant and electron charge, respectively, $\ln\Lambda$ is the Coulomb logarithm, and $\bar{Q}_{e\text{-}e}$ is the averaged Coulomb cross section calculated with an impact parameter cutoff at the Debye length.

It should be emphasized that in some situations T_e does not represent the electron average energy given by $\langle\varepsilon\rangle\approx 3/2kT_e$. In such cases, T_e is just a parameter describing the shape of the electron distribution at low electron energies where $f(\varepsilon)$ is close to Maxwellian (see below). Therefore the parameter T_e, called in the present work "electron temperature," appears only in collision integral for the electron-electron scattering. Using T_e for this purpose is justified because the electron-electron collisions are the most effective at low energies where the electron distribution is always close to Maxwellian.

Electron–heavy-particle elastic collisions

The collision term for the electron–heavy-particle interactions is a sum of the terms for electron-atom and electron-ion collisions,

$$\left[\frac{\delta f}{\delta t}\right]_{e\text{-}h}=\left[\frac{\delta f}{\delta t}\right]_{e\text{-}a}+\left[\frac{\delta f}{\delta t}\right]_{e\text{-}+}, \tag{22}$$

where

$$\left[\frac{\delta f}{\delta t}\right]_{e\text{-}a}=N_e(2\varepsilon/m_e)^{1/2}\frac{1}{\varepsilon}\frac{d}{d\varepsilon}\times\left[a_a(\varepsilon)\left[kT_a\frac{df(\varepsilon)}{d\varepsilon}+f(\varepsilon)\right]\right], \tag{23}$$

$$\left[\frac{\delta f}{\delta t}\right]_{e\text{-}+}=N_e(2\varepsilon/m_e)^{1/2}\frac{1}{\varepsilon}\frac{d}{d\varepsilon}\times\left[a_+(\varepsilon)\left[kT_+\frac{df(\varepsilon)}{d\varepsilon}+f(\varepsilon)\right]\right], \tag{24}$$

$$a_a(\varepsilon)=\frac{2m_eN_1}{m_aN_e}Q_{e\text{-}a}(\varepsilon)\varepsilon^2, \tag{25}$$

$$a_+(\varepsilon)=\frac{2m_eN_1}{m_+N_+}Q_{e\text{-}+}(\varepsilon)\varepsilon^2, \tag{26}$$

m_a and m_+ are masses of the helium atom and the ground-state ion, respectively, N_1 and N_+ are atomic and ionic ground-state densities, respectively, $Q_{e\text{-}a}$ is the electron-atom momentum transfer cross section[16] and $Q_{e\text{-}+}$ is the electron-ion momentum transfer cross section,

$$Q_{e\text{-}+}(\varepsilon)=\frac{\pi e^4}{\varepsilon^2}\ln\Lambda. \tag{27}$$

We assume throughout this work that the ionic temperature $T_+=T_a$.

Electron-impact excitation

Since we consider three-level atoms this collision term takes into account only $1\rightleftarrows 2$ electron-impact transitions. Using the principle of detailed balance,

$$Q_{21}(\varepsilon)=\frac{g_1}{g_2}\frac{\varepsilon+\varepsilon_{12}}{\varepsilon}Q_{12}(\varepsilon+\varepsilon_{12}), \tag{28}$$

the excitation collision term is

$$\left[\frac{\delta f}{\delta t}\right]_{\text{exc}}=-(2\varepsilon/m_e)^{1/2}N_1\left[Q_{12}(\varepsilon)\left[f(\varepsilon)-\frac{N_2}{N_1}\frac{g_1}{g_2}f(\varepsilon-\varepsilon_{12})\right]+Q_{12}(\varepsilon+\varepsilon_{12})\frac{(\varepsilon+\varepsilon_{12})}{\varepsilon}\left[\frac{N_2}{N_1}\frac{g_1}{g_2}f(\varepsilon)-f(\varepsilon+\varepsilon_{12})\right]\right], \tag{29}$$

where $Q_{12}(\varepsilon)$ is the excitation cross section for the $1\rightarrow 2$ transition and N_i and g_i are density and statistical weight of the ith level, respectively.

Electron-impact ionization

We introduce differential ionization cross section $\sigma_{ic}(\varepsilon,\varepsilon',\varepsilon_b)$ and differential recombination cross section $\sigma_{ci}(\varepsilon',\varepsilon_b,\varepsilon)$ defined in the following way: $\sigma_{ic}(\varepsilon,\varepsilon',\varepsilon_b)$ is the differential cross section for the ionization of an atom from the ith level by an electron of energy ε, resulting in an ejected electron of energy ε_b and $\sigma_{ci}(\varepsilon',\varepsilon_b,\varepsilon)$ is the differential cross section for the reverse process. Then, the number of ionizations per unit volume and unit time produced by electrons with energies in the range $[\varepsilon,\ \varepsilon+d\varepsilon]$ such that after the collision the two outgoing electrons have energies in the ranges $[\varepsilon',\ \varepsilon'+d\varepsilon']$ and $[\varepsilon_b,\ \varepsilon_b+d\varepsilon_b]$, respectively, is

$$N_iN_e(2\varepsilon/m_e)^{1/2}f(\varepsilon)\sigma_{ic}(\varepsilon,\varepsilon',\varepsilon_b)d\varepsilon\,d\varepsilon'd\varepsilon_b, \tag{30}$$

and the number of the corresponding three-body recombinations per unit volume and unit time is

$$N_+N_e^2(2\varepsilon'/m_e)^{1/2}(2\varepsilon_b/m_e)^{1/2}f(\varepsilon')f(\varepsilon_b)\sigma_{ci}(\varepsilon',\varepsilon_b,\varepsilon)d\varepsilon'd\varepsilon_bd\varepsilon. \tag{31}$$

Using the Fowler relationship,[17]

$$g_i \varepsilon \sigma_{ic}(\varepsilon,\varepsilon',\varepsilon_b)=\frac{16\pi m_e}{h^3} g_+ \varepsilon' \varepsilon_b \sigma_{ci}(\varepsilon',\varepsilon_b,\varepsilon) , \tag{32}$$

and summing over all energies ε' one obtains the following collision term for the electron-impact ionization and three-body recombination:

$$\left[\frac{\delta f}{\delta t}\right]_{\text{ion}} = -(2\varepsilon/m_e)^{1/2} \sum_{i=1}^{2} \left[N_i Q_{ic}(\varepsilon) f(\varepsilon) - N_e N_+ \frac{C_i}{2} \int_0^{\varepsilon - U_i} \sigma_{ic}(\varepsilon,\varepsilon_b) f(\varepsilon_b) f(\varepsilon - U_i - \varepsilon_b) d\varepsilon_b \right] , \tag{33}$$

where

$$C_i = \frac{g_i}{2\pi g_e g_+} \left[\frac{h^2}{2m_e}\right]^{3/2} , \tag{34}$$

and Q_{ic}, the electron-impact ionization cross section for an atom excited to the ith level, is related to the differential cross section $\sigma_{ic}(\varepsilon,\varepsilon_b)$ through the following relationship:

$$Q_{ic}(\varepsilon) = \tfrac{1}{2} \int_0^{\varepsilon - U_i} \sigma_{ic}(\varepsilon,\varepsilon_b) d\varepsilon_b . \tag{35}$$

Photoionization

The collisional term associated with photoionization can be written

$$\left[\frac{\delta f}{\delta t}\right]_{\text{ph}} = -\sum_i^2 \frac{N_i}{N_e} \frac{4\pi}{h^2 \nu} \frac{\sigma_{ic}(\nu)}{\varepsilon^{1/2}} \times \left[\frac{N_i^*}{N_i} \frac{f(\varepsilon)}{f^*(\varepsilon)} \left[\frac{2h\nu^3}{c^2} + J_\nu \right] \times e^{-h\nu/kT_e} - J_\nu \right] , \tag{36}$$

where $\sigma_{ic}(\nu)$ is the photoionization cross section for the ith level, J_ν is the mean intensity of radiation, $h\nu = \varepsilon + U_i$, and N_i^* is given by the Saha equation,

$$N_i^* = N_e N_+ \left[\frac{h^2}{2\pi m_e k T_e}\right]^{3/2} \frac{g_i}{g_e g_+} \exp(U_i/kT_e) . \tag{37}$$

Radiative recombination

In this case the collisional term is

$$\left[\frac{\delta f}{\delta t}\right]_{\text{RR}} = (2\varepsilon/m_e)^{1/2} \sum_{i=1}^{2} N_+ f(\varepsilon) \sigma_{ci}(\varepsilon) , \tag{38}$$

where $\sigma_{ci}(\varepsilon)$ is the radiative recombination cross section for the $c \rightarrow i$ transition.

Penning ionization

The maximum energy of the electrons produced in process (1) is the difference between twice the energy ε_{12} and the atomic ionization energy U_1. This difference, $(\varepsilon_{\text{PI}})_{\max}$, is 15.05 eV. Since process (1) produces three particles, the ejected electron can have energy in the range $0 \le \varepsilon \le 15.05$ eV. The probability per unit interval of energy of producing these electrons with energy $[\varepsilon, \varepsilon + d\varepsilon]$ was found[18] to be proportional to $\varepsilon^{1/2}[(\varepsilon_{\text{PI}})_{\max} - \varepsilon]^{3/2}$. Then, the normalized energy distribution of the ejected electrons is

$$f_{\text{PI}}(\varepsilon) = C_p [(\varepsilon_{\text{PI}})_{\max} - \varepsilon]^{3/2} , \tag{39}$$

with the normalization constant

$$C_p = \frac{16}{\pi (\varepsilon_{\text{PI}})_{\max}^3} . \tag{40}$$

Taking the above into account, the collision term for the Penning ionization can be written as

$$\left[\frac{\delta f}{\delta t}\right]_{\text{PI}} = \frac{S_{\text{PI}}(T_a) N_2^2}{2N_e} f_{\text{PI}}(\varepsilon), \quad 0 \le \varepsilon \le 15.05 \text{ eV} \tag{41}$$

where $S_{\text{PI}}(T_a)$ is the corresponding rate coefficient.

Associative ionization

The electrons produced in process (2) will have an energy distribution that depends on the distribution of vi-

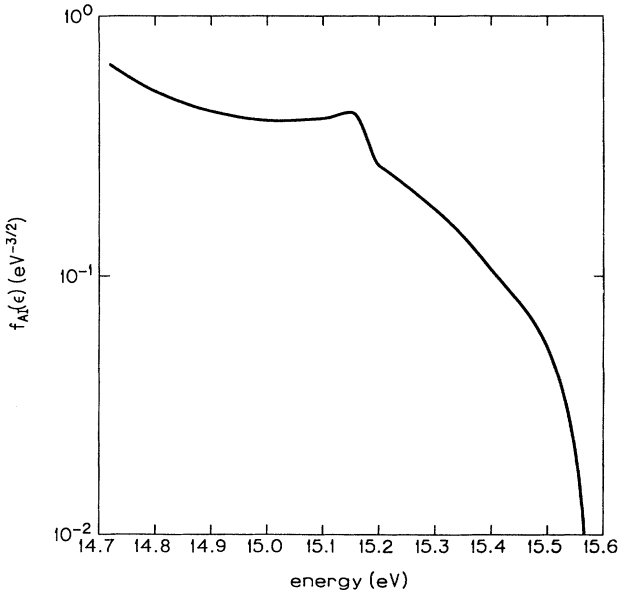

FIG. 1. The ejected electron energy distribution for the associative ionization in helium.

brational and rotational levels of the molecular ions. For the impact energy of 0.03 eV, Garrison *et al.*[19] have shown that the energy of the electrons ranges from 14.7 to 15.6 eV and that the resultant molecular ions are highly vibrationally excited. Using the energy distribution $f_{\mathrm{AI}}(\varepsilon)$ proposed in Ref. 19 (see Fig. 1), the collision term for the associative ionization is

$$\left[\frac{\delta f}{\delta t}\right]_{\mathrm{AI}}=\frac{S_{\mathrm{AI}}(T_a)N_2^2}{2N_e}f_{\mathrm{AI}}(\varepsilon),\quad 14.7\le\varepsilon\le 15.6\ \mathrm{eV} \tag{42}$$

where $S_{\mathrm{AI}}(T_a)$ is the rate coefficient for the process.

Atom-impact ionization

Production of electrons through the atom-impact processes (9) and (10) can be significant in plasmas of high T_a and low ionization degree.[20] However, (1) lack of data on the ionizing collisions of the metastable atoms, (2) uncertainty associated with the threshold behavior of the ionization cross sections for collisions of the ground-state atoms,[21] and (3) lack of data on the energy distribution of the ejected electrons[21] do not allow for a reliable estimate of the contribution of processes (9) and (10) to the production of plasma electrons.

Diffusion term

The diffusion loss of the electrons is taken into account by including the following diffusion term:

$$\left[\frac{\delta f}{\delta t}\right]_{\mathrm{diffusion}}=-\frac{f(\varepsilon)}{\tau_D(\varepsilon)}\ , \tag{43}$$

where τ_D is the electron diffusion time. Assuming "free" diffusion and that the reflection coefficients of the fast electrons at the wall are zero, the diffusion time of the electrons to the wall in a cylindrical tube is

$$\tau_D(\varepsilon)=\frac{r^2}{5.8D(\varepsilon)}\ , \tag{44}$$

where r is the radius of the tube, the electron diffusion coefficient D is

$$D(\varepsilon)=\frac{2\varepsilon}{3m_e\nu_{e\text{-}a}(\varepsilon)}\ , \tag{45}$$

and $\nu_{e\text{-}a}(\varepsilon)$ is the electron-atom elastic collision frequency,

$$\nu_{e\text{-}a}(\varepsilon)=\left[\frac{2\varepsilon}{m_e}\right]^{1/2}N_1Q_{e\text{-}a}(\varepsilon)\ . \tag{46}$$

SIMPLIFICATION OF THE COLLISION TERMS

Electron–heavy-particle elastic collisions

Since

$$\frac{Q_{e\text{-}+}}{Q_{e\text{-}e}}=\frac{3}{2}\left[\frac{kT_e}{\varepsilon}\right]^2\ , \tag{47}$$

the ratio of the electron-ion scattering term to the electron-electron scattering term is equal to about m_e/m_+ and the former term can be neglected.

We include in our analysis the collision term for the electron-atom elastic scattering because this term is of some importance in dense, weakly ionized helium plasmas [the momentum transfer cross section for the e-He scattering is almost constant up to $\varepsilon\approx 20$ eV and is relatively large[16] (about 6×10^{-16} cm^2)]. Taking this into account, the collision term for the electron–heavy-particle interactions can be given by its electron-atom part,

$$\left[\frac{\delta f}{\delta t}\right]_{e\text{-}h}=N_e(2\varepsilon/m_e)^{1/2}\frac{1}{\varepsilon}\frac{d}{d\varepsilon}\times\left[a_a(\varepsilon)\left[kT_a\frac{df(\varepsilon)}{d\varepsilon}+f(\varepsilon)\right]\right]\ . \tag{48}$$

Electron-impact ionization

The electron distribution has very small values when the electron energy exceeds the ionization potential U_1 by more than several kT_e. In addition, the energies ε_b of the secondary electrons ejected during the $1\rightarrow c$ ionization are much smaller (order of kT_e) than U_1.[22,23] Therefore one can assume that

$$f(\varepsilon_b)\approx f^*(\varepsilon_b)\ . \tag{49}$$

The postcollision energies of the incident electrons are also relatively small and their distribution can be approximated by

$$f^*(\varepsilon_b)f^*(\varepsilon'=\varepsilon-U_1-\varepsilon_b)\approx(2/\sqrt{\pi})(kT_e)^{-3/2}\times\exp(U_1/kT_e)f^*(\varepsilon)\ . \tag{50}$$

Using the above, one can write the collision term for the electron-impact ionization of the ground-state atoms,

$$\left[\frac{\delta f}{\delta t}\right]_{\mathrm{ion}}^{(1)}=-(2\varepsilon/m_e)^{1/2}\times\left[N_1Q_{1c}(\varepsilon)f(\varepsilon)-N_eN_+C_1Q_{1c}(\varepsilon)\times\frac{2f^*(\varepsilon)\exp(U_1/kT_e)}{\sqrt{\pi}(kT_e)^{3/2}}\right]\ , \tag{51}$$

and for the electron-impact ionization of the He($2\,^3S_1$) atoms,

$$\left[\frac{\delta f}{\delta t}\right]_{\mathrm{ion}}^{(2)}=-(2\varepsilon/m_e)^{1/2}\times\left[N_2Q_{2c}(\varepsilon)f(\varepsilon)-N_eN_+C_2Q_{2c}(\varepsilon)\times\frac{2f^*(\varepsilon)\exp(U_2/kT_e)}{\sqrt{\pi}(kT_e)^{3/2}}\right]\ . \tag{52}$$

Photoionization

The ratio of the photoionization collision term to the Coulomb scattering term is of orders of magnitude smaller than one[3] so that the photoionization collision term can be neglected in all realistic situations.

Radiative recombination

It was shown by Shaw, Mitchner, and Kruger[4] that the radiative recombination terms are negligible, when compared to other terms, in all practical situations.

INELASTIC CROSS SECTIONS AND RATE COEFFICIENTS

Electron-impact excitation

The cross section for the $1\rightarrow 2$ electron-impact excitation is taken from the work of Scott and McDowell.[24] Since the electron energy distribution may deviate significantly from the Maxwellian, the corresponding rate coefficient C_{12} is calculated directly from Eq. (17).

Electron-impact ionization

The cross sections for the electron-impact ionization of helium from the ground state and from the first excited state are taken from the work of Janev *et al.*[25] The corresponding ionization rate coefficients are calculated from Eq. (17).

Penning and associative ionization

The rate coefficients for the Penning and associative ionizations at high temperatures are unknown. However, their rates at $T_a=300$ K were estimated as 1.35×10^{-9} and 3.15×10^{-9} cm^3/s, respectively.[26] We assume that the rate coefficients for the Penning ionization are constant in the considered range of T_a and that the rate for the associative ionization has the following temperature dependence:[27]

$$S_{\mathrm{AI}}=3.15\times10^{-9}\left[\frac{300}{T_a}\right]^{3/2}\ \mathrm{cm}^3/\mathrm{s}\ . \tag{53}$$

SOLUTION OF THE BOLTZMANN EQUATION

Taking the above into account the Boltzmann equation (14) can be written as

$$\frac{d^2f(\varepsilon)}{d\varepsilon^2}+A(\varepsilon)\frac{df(\varepsilon)}{d\varepsilon}+B(\varepsilon)f(\varepsilon)+C(\varepsilon)=0 \tag{54}$$

with

$$A(\varepsilon)=\frac{1}{a(\varepsilon)}(a'+b_e+a_a)\ , \tag{55}$$

$$B(\varepsilon)=\frac{1}{a(\varepsilon)}\left[b_e'+a_a'-\frac{g_1}{g_2}\lambda_2(\varepsilon+\varepsilon_{12})Q_{12}(\varepsilon+\varepsilon_{12})-\lambda_2\varepsilon Q_{2c}(\varepsilon)-\lambda_1\varepsilon Q_{12}(\varepsilon)-\lambda_1\varepsilon Q_{1c}(\varepsilon)\right]\ , \tag{56}$$

$$\begin{aligned}C(\varepsilon)=\frac{1}{a(\varepsilon)}\Bigg[&\lambda_1(\varepsilon+\varepsilon_{12})Q_{12}(\varepsilon+\varepsilon_{12})f(\varepsilon+\varepsilon_{12})+\left[\frac{m_e}{2\varepsilon}\right]^{1/2}\frac{S_{\mathrm{PI}}\lambda_2^2\varepsilon f_{\mathrm{PI}}(\varepsilon)}{2}\\&+N_+C_2Q_{2c}(\varepsilon)\frac{2f^*(\varepsilon)\exp(U_2/kT_e)}{\sqrt{\pi}(kT_e)^{3/2}}+\left[\frac{m_e}{2\varepsilon}\right]^{1/2}\frac{S_{\mathrm{AI}}\lambda_2^2\varepsilon f_{\mathrm{AI}}(\varepsilon)}{2}\\&+\frac{g_1}{g_2}\lambda_2\varepsilon Q_{12}(\varepsilon)f(\varepsilon-\varepsilon_{12})+N_+C_1Q_{1c}(\varepsilon)\frac{2f^*(\varepsilon)\exp(U_1/kT_e)}{\sqrt{\pi}(kT_e)^{3/2}}\Bigg]\ ,\end{aligned} \tag{57}$$

where $\lambda_i=N_i/N_e$ and $a(\varepsilon)=a_e(\varepsilon)+a_a(\varepsilon)kT_a$, and the boundary conditions are

$$f(\varepsilon)=f^*(\varepsilon)\quad\text{when } \varepsilon\le kT_e \tag{58}$$

and

$$f(\varepsilon)\rightarrow 0\quad\text{as } \varepsilon\rightarrow\infty\ . \tag{59}$$

The general solution of Eq. (54) for $\varepsilon>kT_e$ can be given by

$$f(\varepsilon)=\alpha_-f^-(\varepsilon)+\alpha_+f^+(\varepsilon)+f_p(\varepsilon)\ , \tag{60}$$

where $f^-(\varepsilon)$ and $f^+(\varepsilon)$ are two linearly independent solutions of the homogeneous equation (54) with α_+ equal to zero since $f^+(\varepsilon)\rightarrow\infty$, as $\varepsilon\rightarrow\infty$. The particular solution, obtained by variation of parameters, is

$$\begin{aligned}f_p(\varepsilon)=&f^-(\varepsilon)\int_0^{\varepsilon}\frac{f^+(t)C(t)}{W(t)}dt\\&+f^+(\varepsilon)\int_{\varepsilon}^{\infty}\frac{f^-(t)C(t)}{W(t)}dt\ ,\end{aligned} \tag{61}$$

where $C(t)$ is given by Eq. (57) and the Wronskian of the homogeneous equation is

$$\begin{aligned}W(t)=&f'^+f^--f^+f'^-\\=&\frac{2}{\sqrt{\pi}(kT_e)^{3/2}}\frac{\exp\{2[X(t)+Y(t)]\}}{a(t)}\ ,\end{aligned} \tag{62}$$

with $X(r)$ and $Y(t)$ defined in Eq. (70).

The nonlinearity of Eq. (54) associated with the Fokker-Planck term is weak because the major contributions of the integrals in $a_e(\varepsilon)$ and $b_e(\varepsilon)$ come from the

low-energy electrons. Therefore one can use the following approximation:[3]

$$\int_0^{\varepsilon}\varepsilon^{3/2}f(\varepsilon)d\varepsilon+\varepsilon^{3/2}\int_{\varepsilon}^{\infty}f(\varepsilon)d\varepsilon \approx \tfrac{3}{2}kT_e\int_0^{\varepsilon}\varepsilon^{1/2}f^*(\varepsilon)d\varepsilon\ , \quad (63)$$

and consequently,

$$a_e(\varepsilon)\approx 3(kT_e)^3\bar{Q}_{e\text{-}e}\int_0^{\varepsilon}\varepsilon^{1/2}f^*(\varepsilon)d\varepsilon \quad (64)$$

and

$$b_e(\varepsilon)\approx 3(kT_e)^2\bar{Q}_{e\text{-}e}\int_0^{\varepsilon}\varepsilon^{1/2}f^*(\varepsilon)d\varepsilon\ . \quad (65)$$

Numerical solution

Direct numerical solution of Eq. (54) in the entire range of energy is not possible due to the presence of the exponentially growing mode of the solution $[f^+(\varepsilon)]$; at high energy it will dominate and filter out all the other modes of the solution. Therefore the numerical solution is divided into two parts. In the low-energy part ($kT_e \lesssim \varepsilon \lesssim U_2$), the numerical solution of Eq. (54) (with the boundary condition at kT_e) is obtained by Gear's method; the fact that Eq. (54) can be stiff has to be taken into consideration. (One should add that at these energies both growing and decaying modes of the solution are probable.) The low-energy part of the solution is taken as the starting point for both numerical and WKB solutions (see below) of Eq. (54) at higher energies ($\varepsilon > U_2$). In the high-energy part, an efficient semianalytical procedure[3] is used since the growing mode of the solution filters out the other modes. First, one lets $f^+(\varepsilon)$ be one of the linearly independent homogeneous solutions obtained by Gear's method with initial conditions imposed on f^+ and $df^+/d\varepsilon$ at U_2. Then, a second linearly independent homogeneous solution, say $f^-(\varepsilon)$, can be obtained from

$$f^-(\varepsilon)=f^+(\varepsilon)\int_{\varepsilon}^{\infty}\frac{W(t)}{[f^+(t)]^2}dt\ . \quad (66)$$

Finally, the particular solution can be constructed from the two linearly independent homogeneous solutions and the complete solution can be given by Eq. (60) (with the boundary condition at $\varepsilon=U_2$ taken from the low-energy solution).

The WKB solution

In general, an analytical solution of homogeneous equation (54) can be given by the WKB approximation. This is done by using

$$f^{\pm}(\varepsilon)=\frac{\exp[X(\varepsilon)+Y(\varepsilon)]}{\sqrt{a(\varepsilon)}}h^{\pm}(\varepsilon) \quad (67)$$

to transform the homogeneous part of Eq. (54) into

$$\frac{d^2h}{d\varepsilon^2}-p(\varepsilon)h=0,\quad \varepsilon\geq U_2\ , \quad (68)$$

where, in our case,

$$p(\varepsilon)=\frac{a''}{2a}-\left[\frac{a'}{2a}\right]^2+\frac{b_e+a_a}{a}\left[\frac{a'}{2a}\right] -\frac{b_e+a_a}{a}(X'+Y')-(X''+Y'') -(X'+Y')^2-B(\varepsilon) \quad (69)$$

and

$$X(\varepsilon)=-\tfrac{1}{2}\int_0^{\varepsilon}\frac{b_e(t)}{a(t)}dt,\quad Y(\varepsilon)=-\tfrac{1}{2}\int_0^{\varepsilon}\frac{a_a(t)}{a(t)}dt\ . \quad (70)$$

It should be noted that the function $p(\varepsilon)$ is positive for $\varepsilon \gtrsim U_2$ in plasmas considered here, with the requirement that

$$|R(\varepsilon)|=\left|\frac{4pp''-5(p')^2}{16p^3}\right|=\left|-\frac{1}{p^{3/2}}\frac{d^2}{d\varepsilon^2}\left[\frac{1}{p^{1/4}}\right]\right|\ll 1\ . \quad (71)$$

The general solutions of Eq. (68) are

$$h^{\pm}(\varepsilon)=p(\varepsilon)^{-1/4}\exp\left[\pm\int_{\varepsilon_{\min}}^{\varepsilon}p(t)^{1/2}dt\right](1+\delta_{\pm})\ , \quad (72)$$

where $\delta_{\pm}$ are the upper bounds, discussed below, of the error of the WKB approximation.

Since $p(\varepsilon)$ has discontinuities around the thresholds for the inelastic processes, the WKB solution for $h^{\pm}(\varepsilon)$ is given in the following three intervals:

I, $\varepsilon_{\min}=U_2\leq\varepsilon\leq\varepsilon_{\max}=\varepsilon_{12}$:

$$h_{\rm I}^{+}(\varepsilon)=p(\varepsilon)^{-1/4}[K_{\rm I}S_{\rm I}(\varepsilon)],\quad K_{\rm I}=1\ , \quad (73)$$

$$h_{\rm I}^{-}(\varepsilon)=p(\varepsilon)^{-1/4}[J_{\rm I}S_{\rm I}^{-1}(\varepsilon)]\ , \quad J_{\rm I}=J_{\rm II}S_{\rm I}(\varepsilon_{12})S_{\rm II}^{-1}(\varepsilon_{12})\ , \quad (74)$$

II, $\varepsilon_{\min}=\varepsilon_{12}\leq\varepsilon\leq\varepsilon_{\max}=U_1$:

$$h_{\rm II}^{+}(\varepsilon)=p(\varepsilon)^{-1/4}[K_{\rm II}S_{\rm II}(\varepsilon)]\ , \quad K_{\rm II}=K_{\rm I}S_{\rm I}(\varepsilon_{12})S_{\rm II}^{-1}(\varepsilon_{12})\ , \quad (75)$$

$$h_{\rm II}^{-}(\varepsilon)=p(\varepsilon)^{-1/4}[J_{\rm II}S_{\rm II}^{-1}(\varepsilon)]\ , \quad J_{\rm II}=J_{\rm III}S_{\rm II}(U_1)S_{\rm III}^{-1}(U_1)\ , \quad (76)$$

III, $\varepsilon_{\min}=U_1\leq\varepsilon\leq\varepsilon_{\max}=2U_1$:

$$h_{\rm III}^{+}(\varepsilon)=p(\varepsilon)^{-1/4}[K_{\rm III}S_{\rm III}(\varepsilon)]\ , \quad K_{\rm III}=K_{\rm II}S_{\rm II}(U_1)S_{\rm III}^{-1}(U_1)\ , \quad (77)$$

$$h_{\rm III}^{-}(\varepsilon)=p(\varepsilon)^{-1/4}[J_{\rm III}S_{\rm III}^{-1}(\varepsilon)]\ , \quad J_{\rm III}=\frac{K_{\rm III}^{-1}}{\sqrt{\pi}(kT_e)^{3/2}}\ , \quad (78)$$

where

$$S_i(\varepsilon)=\exp\left[\int_{\varepsilon_{\min}}^{\varepsilon}p(t)^{1/2}dt\right]\ , \quad (79)$$

and K_i and J_i are constant parameters imposed to ensure the continuity in the $h^{\pm}(\varepsilon)$ and $dh^{\pm}(\varepsilon)/d\varepsilon$ at each inelastic threshold.

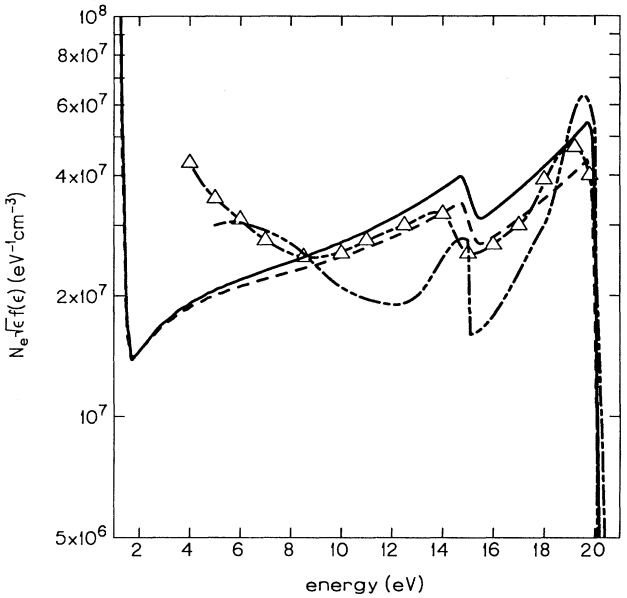

FIG. 2. Comparison of the calculated numerical (solid line) and WKB (dashed line) electron distributions with measured (triangles connected with the dotted-dashed line) electron distribution in helium afterglow experiment ($I=1.8$ A and $P=2$ Torr) of Blagoev *et al.* (Ref. 6). The double-dotted line is the theoretical result of Blagoev *et al.* (Ref. 6). $T_e=1000$ K, $T_a=400$ K, $N_1=4.8\times10^{16}$, $N_2=8\times10^{11}$, and $N_e=4\times10^{12}$ cm^{-3}.

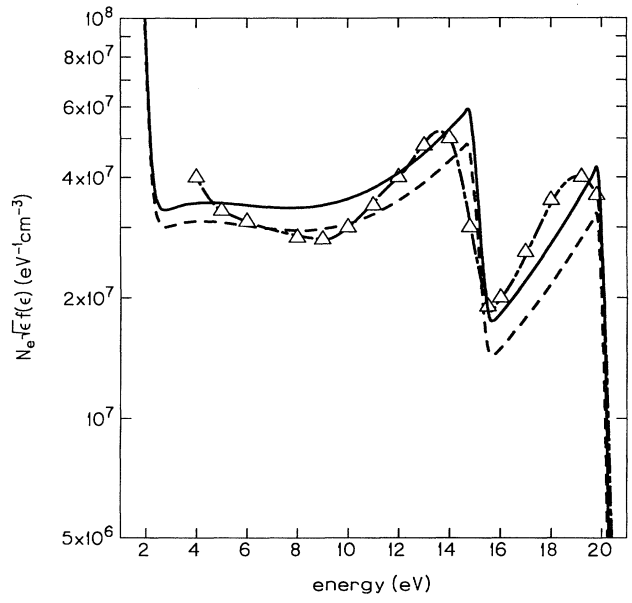

FIG. 3. Comparison of the calculated numerical (solid line) and WKB (dashed line) electron distributions with measured (triangles connected with the dotted-dashed line) electron distribution in helium afterglow experiment ($I=0.45$ A and $P=2$ Torr) of Blagoev *et al.* (Ref. 6). $T_e=1750$ K, $T_a=400$ K, $N_1=4.8\times10^{16}$, $N_2=9\times10^{11}$, and $N_e=1\times10^{12}$ cm^{-3}.

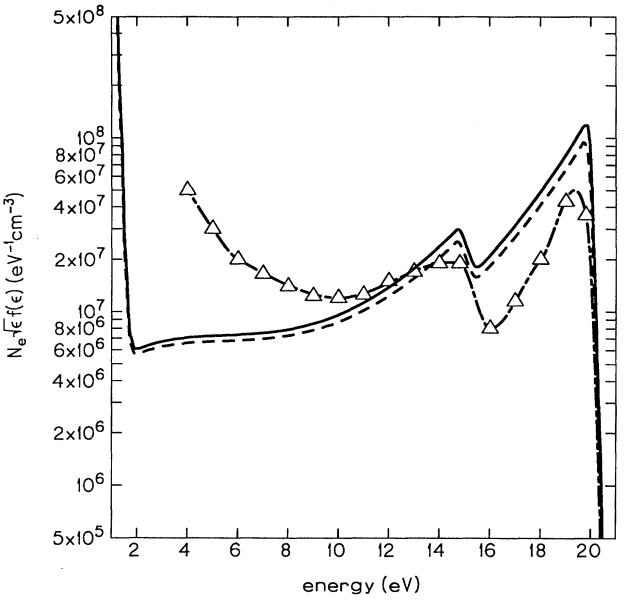

FIG. 4. Comparison of the calculated numerical (solid line) and WKB (dashed line) electron distributions with measured (triangles connected with the dotted-dashed line) electron distribution in helium afterglow experiment ($I=1.8$ A and $P=1$ Torr) of Blagoev *et al.* (Ref. 6). $T_e=1000$ K, $T_a=400$ K, $N_1=2.4\times10^{16}$, $N_2=2.8\times10^{11}$, and $N_e=2\times10^{12}$ cm^{-3}.

RESULTS AND DISCUSSION

The reliability of the numerical and WKB solutions obtained in this work was tested by comparing these solu-

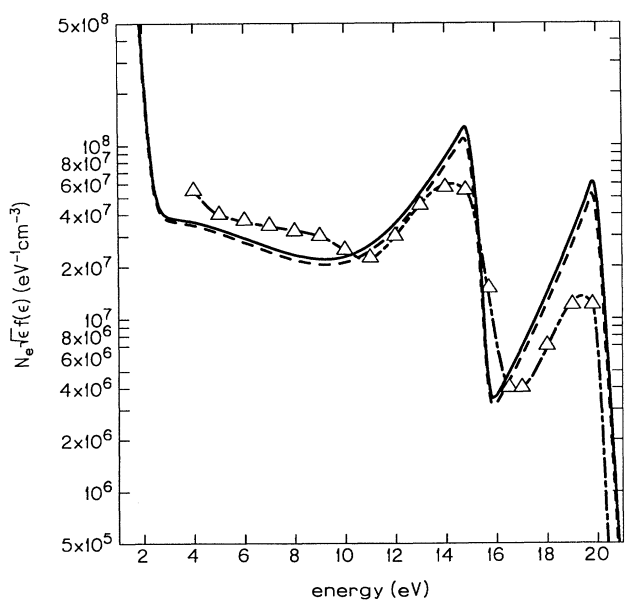

FIG. 5. Comparison of the calculated numerical (solid line) and WKB (dashed line) electron distributions with measured (triangles connected with the dotted-dashed line) electron distribution in helium afterglow experiment ($I=0.45$ A and $P=1$ Torr) of Blagoev *et al.* (Ref. 6). $T_e=2000$ K, $T_a=400$ K, $N_1=2.4\times10^{16}$, $N_2=1\times10^{12}$, and $N_e=6\times10^{11}$ cm^{-3}.

tions with existing measurements of electron distributions in helium afterglow[28,6] (see Figs. 2–5). The comparison shows quite good agreement between the theory and the experiments, except at lower electron energies and higher currents (Figs. 2 and 4). The agreement is in fact better than it appears to be in the figures; the slight differences in the location and width of the fast electron sources (the peaks) result mainly from experimental uncertainties in these regions;[29] the relatively large amplitude of the differentiating signal broadens, especially near the peaks, the measured energy distributions. The discrepancy between the theory and the higher-current experiments in the low-energy region results from the following facts. First, the wall potential in the experiments was not negligible,[29] which retarded the diffusion of the electrons to the wall. In other words, the real diffusion time for the electrons in the experiments was longer than the time obtained under assumption of the "free" diffusion. Unfortunately, introducing a more realistic diffusion time[30] in the treatment of the high-current discharge would limit the applicability of the present approach to particular plasma-wall systems. Therefore we use in the present work the same expression for the electron diffusion in the entire range of the electron energy. This expression has the same r and D dependence as the expression (44) for the "free" diffusion in cylindrical tube but the constant factor 5.8 is replaced by factor 2. Such a procedure seems to be realistic in most situations, especially at high energies. However, it is still inadequate in the high-current discharges (Figs. and 4) at low electron energies. In plasmas with lower values of the electric current, the electron diffusion becomes more "free" like.

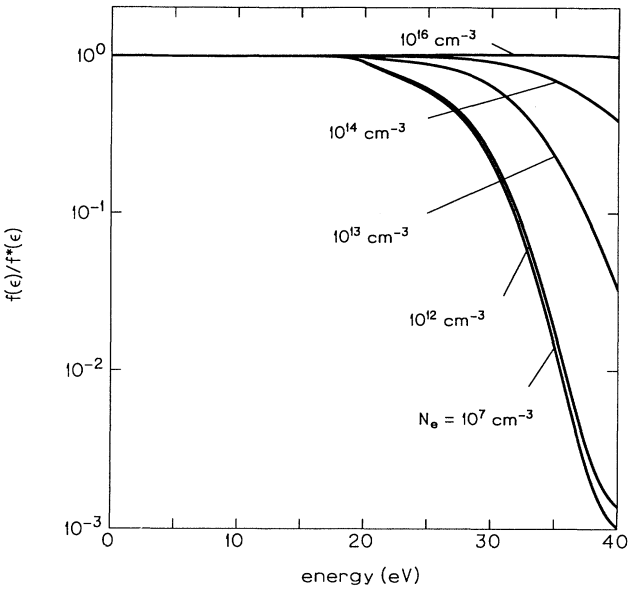

FIG. 7. The calculated (numerical) ratios of the electron distribution to the corresponding Maxwellian distribution. $T_e = 14\,000$ K and $T_a = 14\,000$ K; the values of $(H_{n_{\max}}, B_2)$, are, when N_e varies from 10^7 to 10^{16} cm^{-3}, $(4.5\times10^{-11}, 5.2\times10^{-2})$, $(7.6\times10^{-6}, 6.8\times10^{-2})$, $(3.6\times10^{-4}, 1.2\times10^{-1})$, $(1.9\times10^{-2}, 1.7\times10^{-1})$, and (1, 1), respectively.

The electron distribution was studied in a broad range of conditions: 5000 K $\leq T_a \leq$ 20 000 K, 10 000 K $\leq T_e \leq$ 20 000 K, and 10^{10} cm$^{-3} \leq N_1 \leq 10^{18}$ cm^{-3}. The

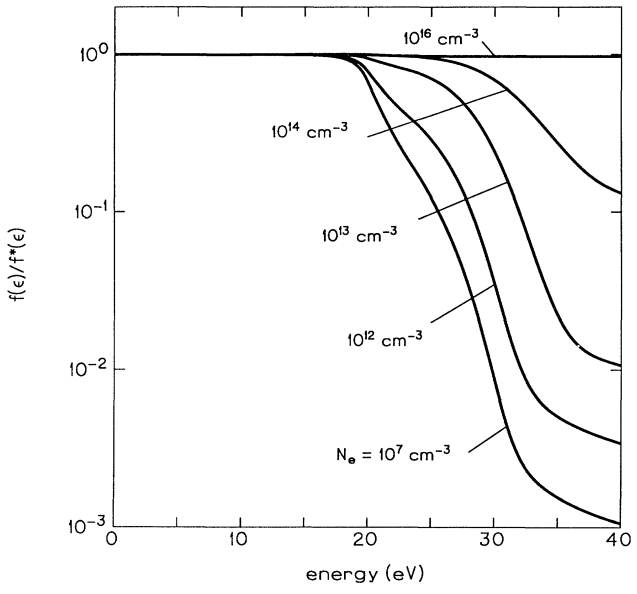

FIG. 6. The calculated (numerical) ratios of the electron distribution to the corresponding Maxwellian distribution. $T_e = 12\,000$ K and $T_a = 12\,000$ K; the values of $(H_{n_{\max}}, B_2)$ are, when N_e varies from 10^7 to 10^{-16} cm^{-3}, $(5.4\times10^{-11}, 5.8\times10^{-2})$, $(3.4\times10^{-5}, 1.9\times10^{-1})$, $(2.2\times10^{-3}, 4.6\times10^{-1})$, $(1.1\times10^{-1}, 7.2\times10^{-1})$, and (1, 1), respectively.

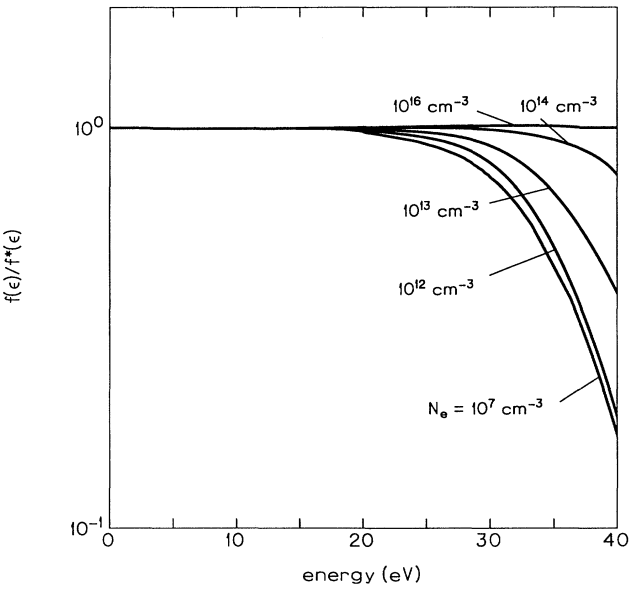

FIG. 8. The calculated (numerical) ratios of the electron distribution to the corresponding Maxwellian distribution. $T_e = 16\,000$ K and $T_a = 16\,000$ K; the values of $(H_{n_{\max}}, B_2)$ are, when N_e varies from 10^7 to 10^{16} cm^{-3}, $(2.0\times10^{-11}, 3.0\times10^{-2})$, $(5.1\times10^{-6}, 5.3\times10^{-2})$, $(1.1\times10^{-4}, 4.9\times10^{-2})$, $(5.8\times10^{-3}, 6.7\times10^{-2})$, and (1, 1), respectively.

nonequilibrium populations of the electrons and the metastable states ($i=2$) are given by, respectively,[31–33]

$$\frac{N_e}{N_1}=\frac{H_{n_{\max}}}{N_+}\frac{g_e g_+}{g_1}\left[\frac{2\pi m_e kT_e}{h^2}\right]^{3/2}\exp\left[-\frac{U_1}{kT_e}\right], \quad (80)$$

$$\frac{N_2}{N_1}=B_2\frac{g_2}{g_1}\exp\left[-\frac{\Delta E_{12}}{kT_e}\right], \quad (81)$$

with factors $H_{n_{\max}}$ and B_2 varying in the following intervals:

$$10^{-14}\le H_{n_{\max}}\le 10^{3} \text{ and } 10^{-3}\le B_2\le 10^{6}, \quad (82)$$

where $H_{n_{\max}}$ is the ratio of the nonequilibrium electron density to the corresponding Saha value and B_2 is the ratio of the nonequilibrium population of the first excited level to the corresponding Boltzmann value.

The steady-state helium plasmas are divided into five categories. The first category includes the cases when $T_e=T_a$. The cases when $T_e\neq T_a$ ($T_e/T_a=1.5$, and 2) are divided into categories A, B, C, and D as follows:

Case	$H_{n_{\max}}<1$	$H_{n_{\max}}\ge 1$	$B_2<1$	$B_2\ge 1$
A	×		×	
B	×			×
C		×	×	
D		×		×

Examples of the electron distribution when $T_e=T_a$ and $H_{n_{\max}}\le 1$ and $B_2\le 1$ (the cases when $T_e=T_a$ and $H_{n_{\max}}$, $B_2>1$ are unrealistic) are given in Figs. 6–8. As can be seen there, the lower limit of T_e (or T_a) above which the electron distribution is close to Maxwellian in the entire range of the considered densities (10^{10} cm$^{-3}\lesssim N_a\lesssim 10^{20}$ cm^{-3}) is about 16000 K. As N_e increases, the role of electron Coulomb collisions becomes more prominent, which brings the tail of the distribution closer to the tail of the Maxwellian distribution. It should be noted that when $H_{n_{\max}}\le 1$ and $B_2\le 1$, only lowering of the tail of the distribution is possible. Also, the solution of the stationary Boltzmann equation for helium with $T_e=T_a$ and $H_{n_{\max}}=1$ and $B_2=1$ gives, as expected, the Maxwellian distribution. The situation when $B_2\approx 1$ is common in stationary plasmas with the lowest excited levels being metastable (for example, in atomic nitrogen and oxygen[31,32]) but rather uncommon in plasmas with the lowest levels being strongly radiative (for example, in atomic argon[1,2] and hydrogen[3,4]).

In case A, $H_{n_{\max}}<1$ and $B_2<1$, the tail of the electron distribution can only be lowered. The deviation of the distribution from Maxwellian is a strong function of the ionization degree. As the ionization degree decreases ($H_{n_{\max}}$ varies from 10^{-6} to 10^{-14}; see Figs. 9 and 10), the presence of the fast electron source at $\varepsilon\approx\varepsilon_{12}$ becomes more apparent since fewer electrons are available to thermalize the fast electrons. Examples of the N_1 dependence of the electron distribution are shown in Figs. 9–12 and the dependence on temperature can be seen in Figs. 9–11. The deviation of the distribution from Maxwellian is less significant at higher temperatures where the ionization degree and the frequency of electron-electron collisions are much higher. The role of the electron-impact ionization and three-body recombination [processes (5)]

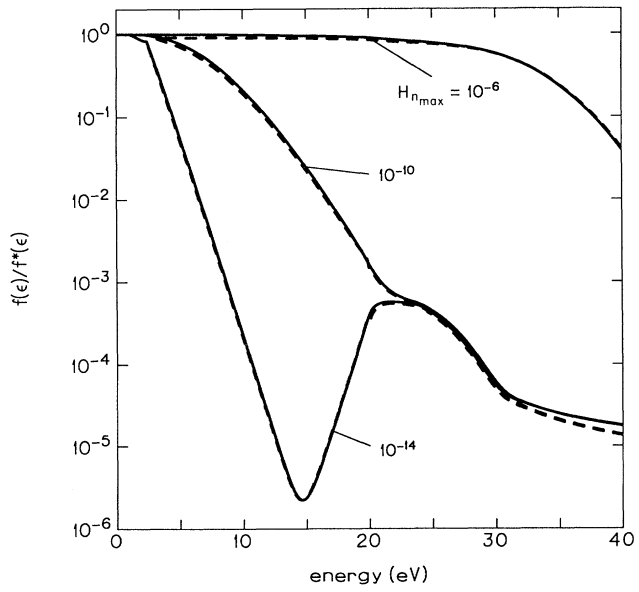

FIG. 9. The calculated (numerical, solid lines and WKB, dashed lines) ratios of the electron distribution to the corresponding Maxwellian distribution. $T_e=10000$ K, $T_a=5000$ K, $N_1=10^{10}$ cm^{-3}, and $B_2=10^{-3}$ (case A).

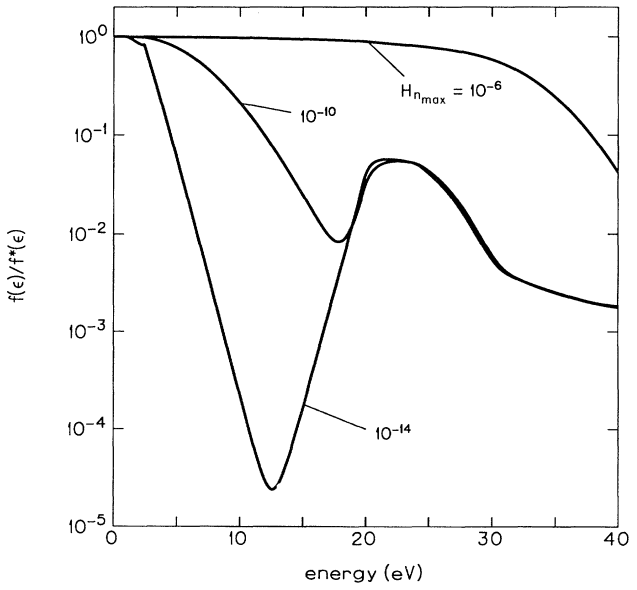

FIG. 10. The calculated (numerical) ratios of the electron distribution to the corresponding Maxwellian distribution. $T_e=10000$ K, $T_a=5000$ K, $N_1=10^{10}$ cm^{-3}, and $B_2=10^{-1}$ (case A).

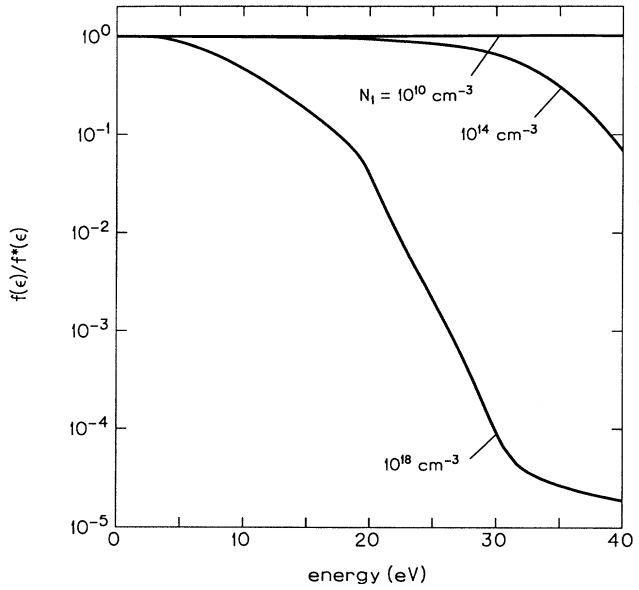

FIG. 11. The calculated (numerical) ratios of the electron distribution to the corresponding Maxwellian distribution. $T_e = 15\,000$ K, $T_a = 10\,000$ K, $H_{n_{max}} = 10^{-6}$, and $B_2 = 10^{-3}$ (case A).

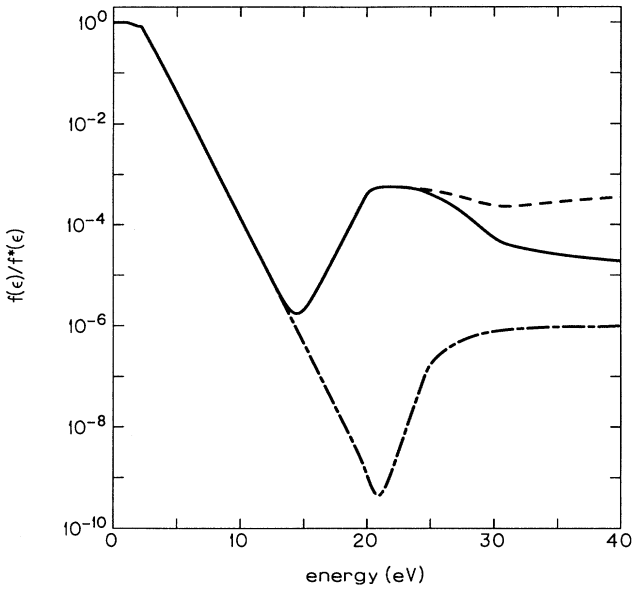

FIG. 12. The calculated (numerical) ratios of the electron energy distribution to the corresponding Maxwellian distribution for $T_e = 10\,000$ K, $T_a = 5000$ K, $N_1 = 10^{18}$ cm^{-3}, $H_{n_{max}} = 10^{-6}$, and $B_2 = 10^{-3}$ (case A). The solid line is the ratio obtained by including all the elastic and inelastic processes; the dashed line is the ratio when the electron-impact ionization from the ground state and the reverse three-body recombination are neglected; the dotted-dashed line is the ratio when the electron-impact deexcitation [process (3)] of the metastable atoms is neglected.

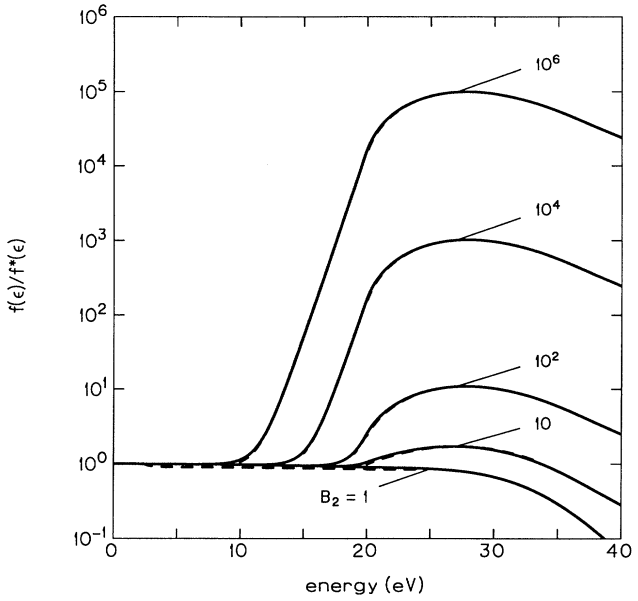

FIG. 13. The calculated (numerical, solid lines and WKB, dashed lines) ratios of the electron distribution to the corresponding Maxwellian distribution for $T_e = 10\,000$ K, $T_a = 5000$ K, $N_1 = 10^{10}$ cm^{-3}, and $H_{n_{max}} = 10^{-6}$ (case B).

and the electron-impact deexcitation [process (3)] in forming the tail of the distribution can be seen in Fig. 12.

In case B, $H_{n_{max}} \geq 1$ and $B_2 \geq 1$, raising of the tail of the electron distribution above the Maxwellian tail is pos-

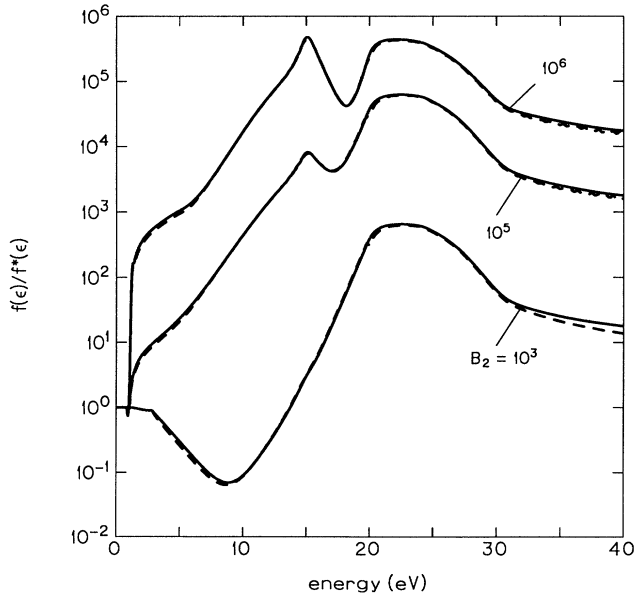

FIG. 14. The calculated (numerical, solid lines and WKB, dashed lines) ratios of the electron distribution to the corresponding Maxwellian distribution for $T_e = 10\,500$ K, $T_a = 7000$ K, $N_1 = 10^{18}$ cm^{-3}, and $H_{n_{max}} = 10^{-6}$ (case B).

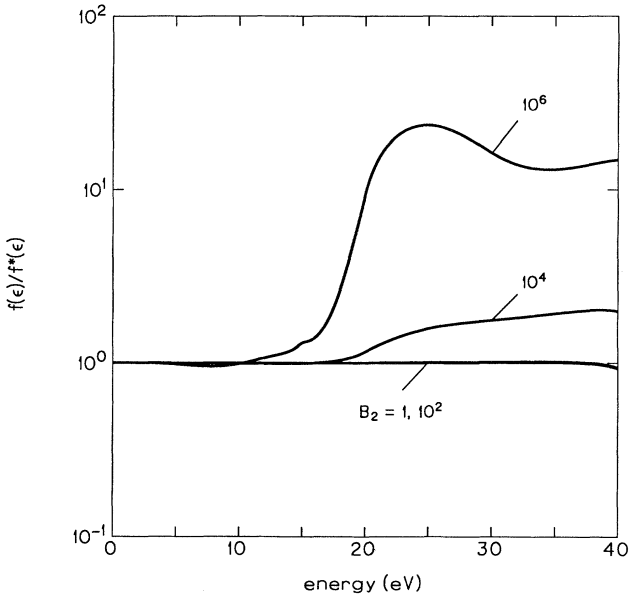

FIG. 15. The calculated (numerical) ratios of the electron distribution to the corresponding Maxwellian distribution for $T_e = 20\,000$ K, $T_a = 10\,000$ K, $N_1 = 10^{10}$ cm^{-3}, and $H_{n_{max}} = 10^{-6}$ (case B).

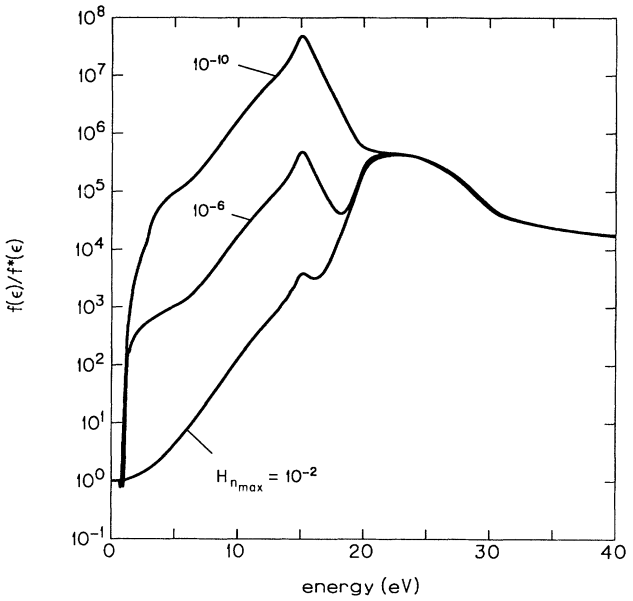

FIG. 17. The calculated (numerical) ratios of the electron distribution to the corresponding Maxwellian distribution for $T_e = 10\,500$ K, $T_a = 7000$ K, $N_1 = 10^{18}$ cm^{-3}, and $B_2 = 10^6$ (case B).

sible. Examples of the dependence of the electron distribution on density (B_2) of the metastable atoms are shown in Figs. 13–15. At a given $H_{n_{max}}$, the tail of the distribution rises with increase of B_2 which is due to the overpopulation of the metastable levels—sources of the fast electrons [processess (1)–(3)]. At a given (high) B_2, the tail of the electron distribution rises rapidly (Figs. 16 and 17) with decrease of the ionization degree (i.e., with worsening of the conditions for electron thermalization). The

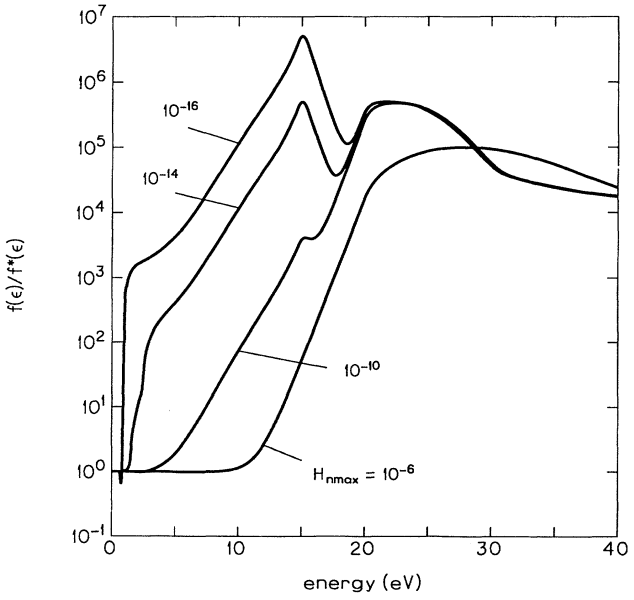

FIG. 16. The calculated (numerical) ratios of the electron distribution to the corresponding Maxwellian distribution for $T_e = 10\,000$ K, $T_a = 5000$ K, $N_1 = 10^{10}$ cm^{-3}, and $B_2 = 10^6$ (case B).

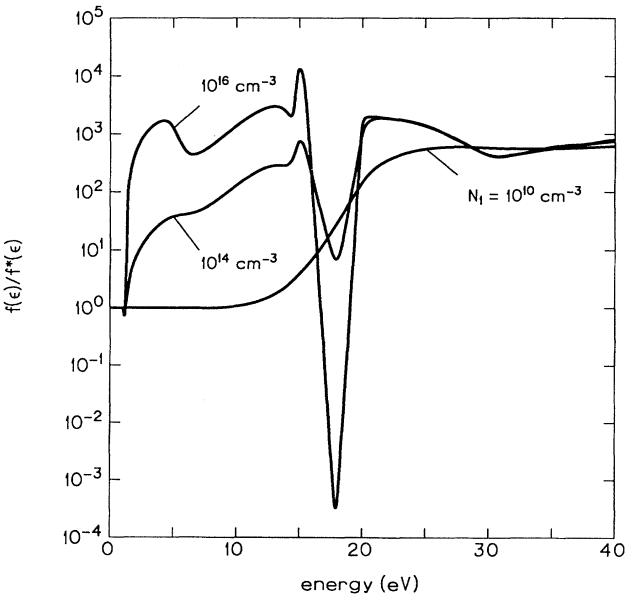

FIG. 18. The calculated (numerical) ratios of the electron distribution to the corresponding Maxwellian distribution for $T_e = 15\,000$ K, $T_a = 10\,000$ K, $H_{n_{max}} = 10^{-6}$, and $B_2 = 10^6$ (case B).

rise of the distribution above the Maxwellian distribution is caused by the collisions of the metastable atoms (Penning and associative ionization), and by the electron-impact deexcitation of the metastables. At low ionization degree, the "humps" on the distributions become more prominent; the hump at $\varepsilon \approx 15$ eV results from the associative ionization, whereas the hump at $\varepsilon \approx \varepsilon_{12}$ results from the electron-impact deexcitation of the metastable atoms. The temperature dependence of the electron distribution can be seen in Figs. 13–18. The magnitude of the rise of the distribution tail is a strong, decreasing function of temperature. Again, this is due to the lesser role of the electron-electron collisions at lower ionization degrees. An interesting example of the N_1 dependence of the ratio $f(\varepsilon)/f^*(\varepsilon)$ at high density of metastable atoms is given in Fig. 18. With increase of the ground-state density at given $H_{n_{\max}}$ and B_2, the rise of the electron distribution, resulting from the presence of the fast electrons produced by processes (1)–(3), becomes very distinctive. At high densities of the ground and the metastable levels, there is a narrow range of energy ($\approx$15–20 eV) where the electron density is very low. Depopulation of the electrons in this region is caused by the electron-impact ionization of the metastable atoms. The role of the ionization of the metastable atoms by electrons can be seen clearly in Fig. 19,

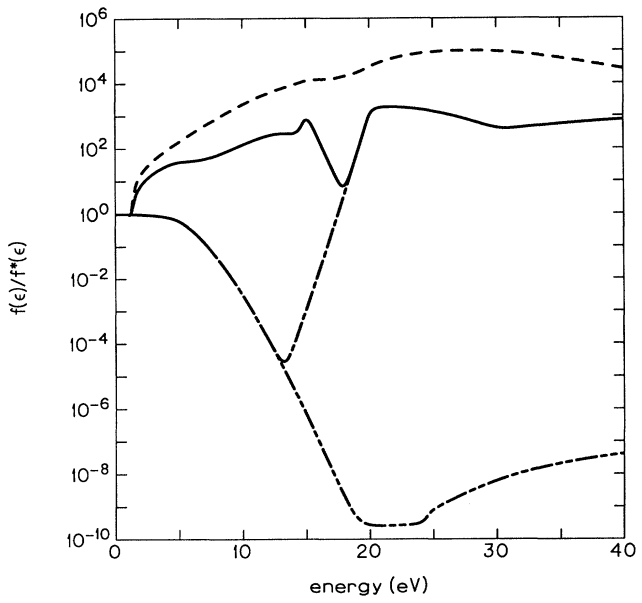

FIG. 19. The calculated (numerical) ratios of the electron energy distribution to the corresponding Maxwellian distribution for $T_e = 15\,000$ K, $T_a = 10\,000$ K, $N_1 = 10^{14}$ cm^{-3}, $H_{n_{\max}} = 10^{-6}$, and $B_2 = 10^6$ (case B). The solid line is the ratio obtained by including all the elastic and inelastic processes; the dashed line is the ratio when the electron-impact ionization from the metastable levels and the reverse three-body recombination are neglected; the dotted-dashed line is the ratio when the associative and the Penning ionization are neglected; the double-dotted-dashed line is the ratio when the associative ionization, the Penning ionization, and the electron-impact deexcitation [process (3)] are neglected.

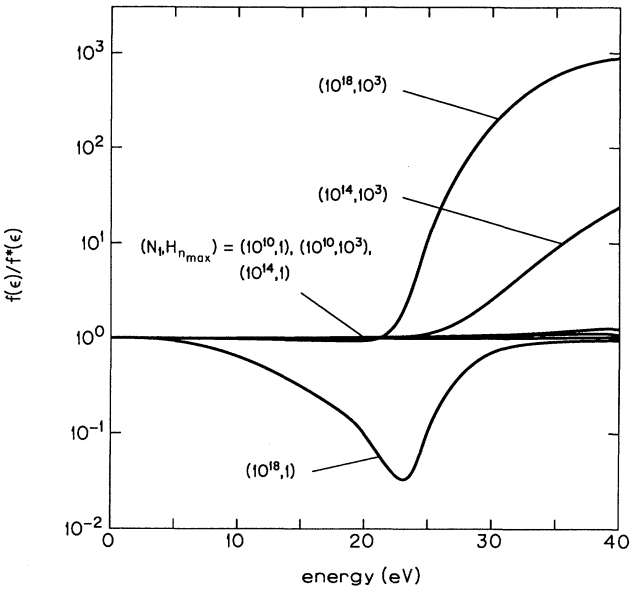

FIG. 20. The calculated (numerical) ratios of the electron distribution to the corresponding Maxwellian distribution for $T_e = 10\,000$ K, $T_a = 5000$ K, and $B_2 = 10^{-3}$ (case C).

where the contributions of the associative and Penning ionizations and process (3) are also shown.

Examples of situations belonging to category C, $H_{n_{\max}} \geq 1$ and $B_2 < 1$, are shown in Fig. 20. The two

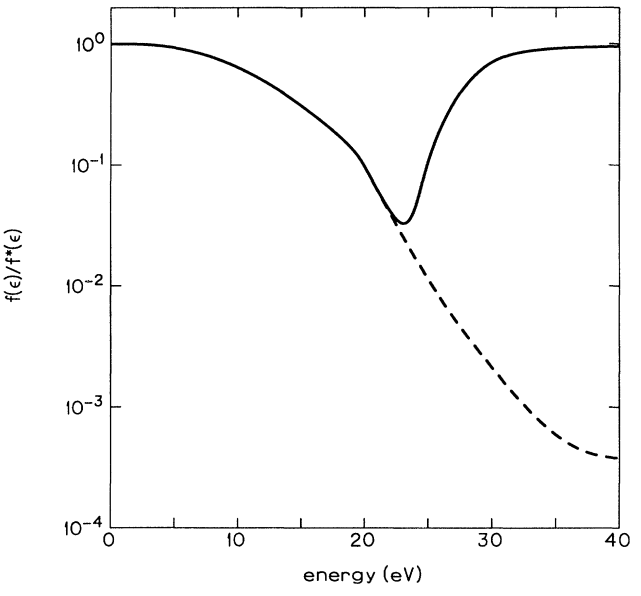

FIG. 21. The calculated (numerical) ratios of the electron energy distribution to the corresponding Maxwellian distribution for $T_e = 10\,000$ K, $T_a = 5000$ K, $N_1 = 10^{18}$ cm^{-3}, $H_{n_{\max}} = 1$, and $B_2 = 10^{-3}$ (case C). The solid line is the ratio obtained by including all the elastic and inelastic processes and the dashed line is the ratio when the electron-impact ionization from the ground state and the reverse three-body recombination are neglected.

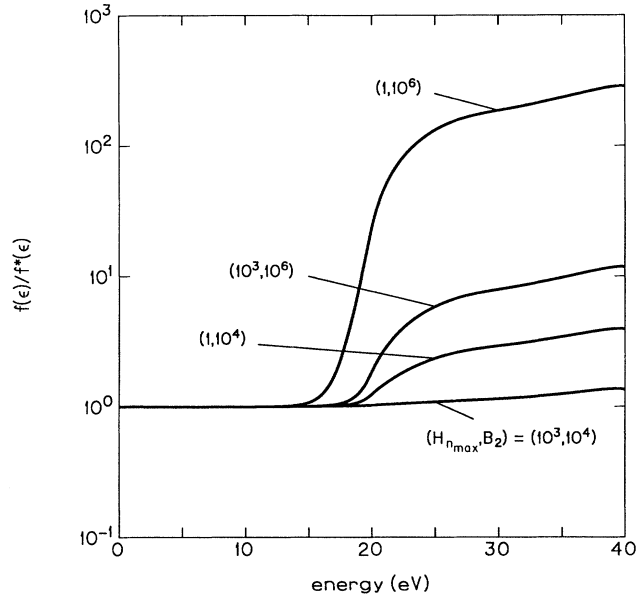

FIG. 22. The calculated (numerical) ratios of the electron distribution to the corresponding Maxwellian distributions for $T_e = 10\,000$ K, $T_a = 5000$ K, and $N_1 = 10^{10}$ cm^{-3} (case D).

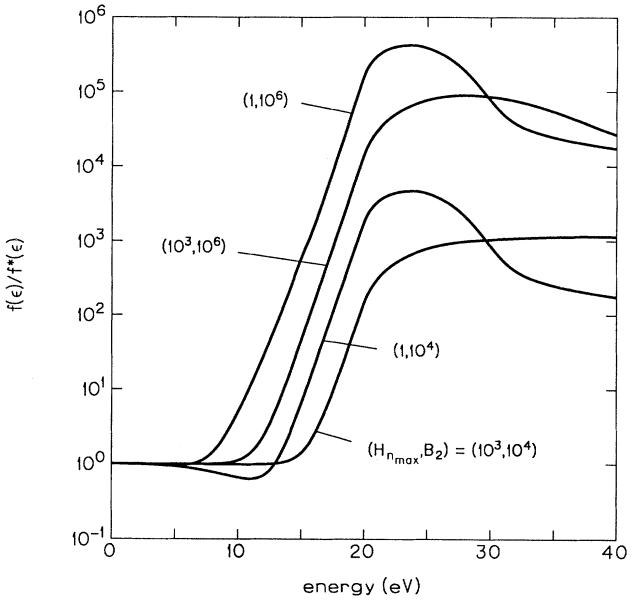

FIG. 24. The calculated (numerical) ratios of the electron distribution to the corresponding Maxwellian distribution for $T_e = 10\,000$ K, $T_a = 5000$ K, and $N_1 = 10^{18}$ cm^{-3} (case D).

upper curves in the figure are characteristic for the conditions when three-body (electron-electron-ion) recombination is effective. This process resupplies the fast electrons lost in the reverse process of ionization and it is effective because the density of electrons under such conditions is very high. The lowest curve in Fig. 20 reflects two trends. The descending part of the distribution results

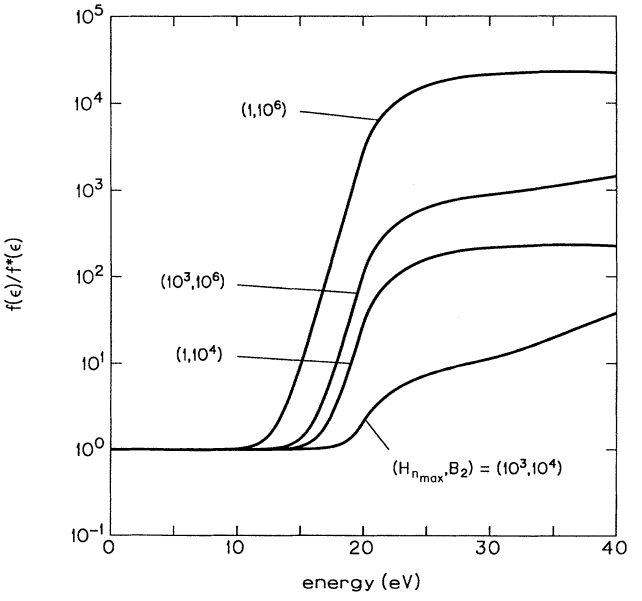

FIG. 23. The calculated (numerical) ratios of the electron distribution to the corresponding Maxwellian distribution for $T_e = 10\,000$ K, $T_a = 5000$ K, and $N_1 = 10^{14}$ cm^{-3} (case D).

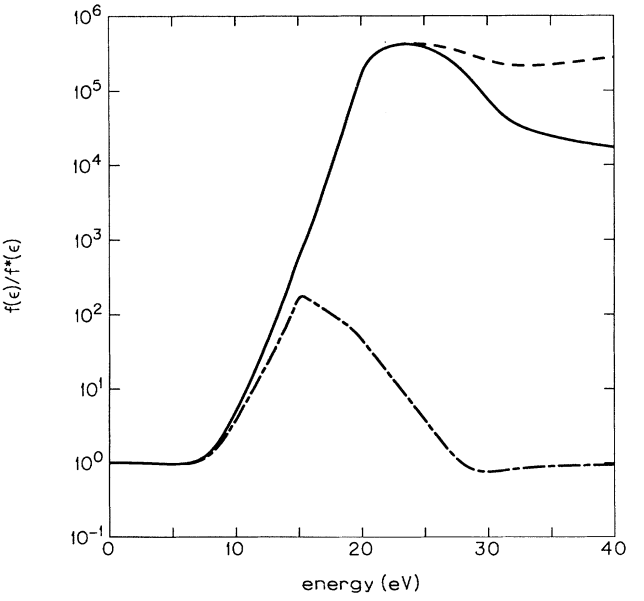

FIG. 25. The calculated (numerical) ratios of the electron energy distribution to the corresponding Maxwellian distribution for $T_e = 10\,000$ K, $T_a = 5000$ K, $N_1 = 10^{18}$ cm^{-3}, $H_{n_{\max}} = 1$, $B_2 = 10^6$ (case D). The solid line is the ratio obtained by including all the elastic and inelastic processes; the dashed line is the ratio when the electron-impact ionization from the ground state and the reverse three-body recombination are neglected; the dotted-dashed line is the ratio when process (3) is neglected.

from the relatively low population of the metastable atoms so that there are not enough electron-impact deexcitations of the metastable atoms to balance the energy lost by electrons in the electron-impact excitation of the metastable atoms. The ascending part of the curve reflects the contribution of the three-body recombination to the ground state. This can also be seen in Fig. 21, where the upper curve represents the situation when all the processes discussed above are included and the lower curve is for the case when the electron-impact ionization of the ground state and the reverse process (three-body recombination) are neglected.

Examples of the electron distribution in case D, $H_{n_{\max}} \geq 1$ and $B_2 \geq 1$, are given in Figs. 22–24. Typically, the tail of the distribution rises above the Maxwellian tail due to the high population of the metastable atoms. This high population causes the rate for the electron-impact deexcitation of the metastables atoms [process (3)] to be very high; the resulting fast electrons overpopulate the tail of the distribution. The N_1 dependence of the electron distribution can be seen from Figs. 22–24. Increase of the ground-state atom density causes a significant decrease of the ionization degree. As a result, the relative role of the electron-electron thermalizing collisions also decreases significantly. The role of the electron-impact ionization of the ground-state atoms in depopulating of the tail of the electron distribution can be seen in Fig. 25, together with the contributions of process (3).

The accuracy of the WKB approximation

The accuracy of the WKB solutions was tested by comparing the WKB results with the numerical solutions of Eq. (54). The differences are within a few percent, except a few extreme situations discussed below. Typical examples of the relative accuracy of the WKB approximation are given in Figs. 26–28. Some of the "bad" cases (those with $B_2 = 10^5, 10^6$) are shown in Fig. 28. One can see that even in such cases, the WKB approach can be used as the

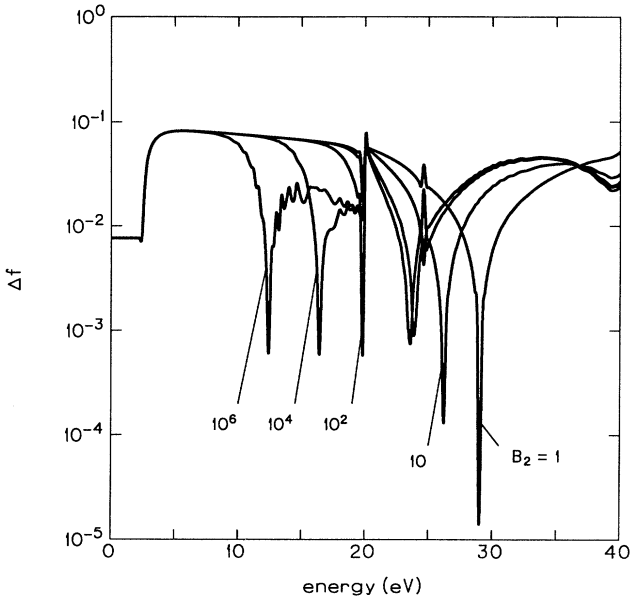

FIG. 27. The relative difference $\Delta f = |(f_{\text{num}} - f_{\text{WKB}})/f_{\text{num}}|$ between the numerical and WKB solutions for $T_e = 10\,000$ K, $T_a = 5000$ K, $N_1 = 10^{10}$ cm^{-3}, and $H_{n_{\max}} = 10^{-6}$ (case B).

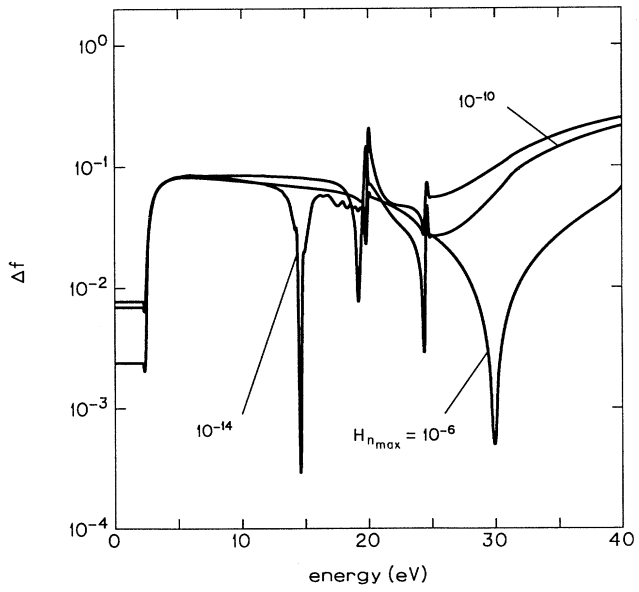

FIG. 26. The relative difference $\Delta f = |(f_{\text{num}} - f_{\text{WKB}})/f_{\text{num}}|$ between the numerical and WKB solutions for $T_e = 10\,000$ K, $T_a = 5000$ K, $N_1 = 10^{10}$ cm^{-3}, and $B_2 = 10^{-3}$ (case A).

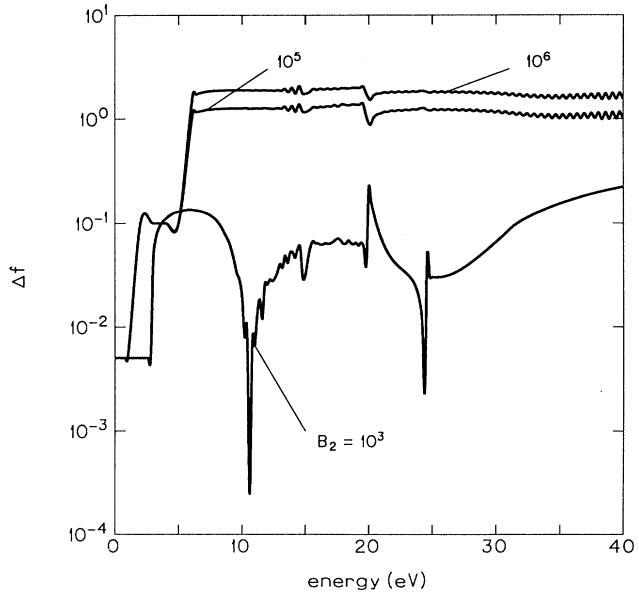

FIG. 28. The relative difference $\Delta f = |(f_{\text{num}} - f_{\text{WKB}})/f_{\text{num}}|$ between the numerical and WKB solutions for $T_e = 10\,500$ K, $T_a = 7000$ K, $N_1 = 10^{18}$ cm^{-3}, and $H_{n_{\max}} = 10^{-6}$ (case B).

first-order approximation to the solution to the stationary electron Boltzmann equation. The reliability of the WKB approximation in plasmas considered here was also suggested in some earlier works.[34–36]

An alternative way of testing the reliability of the WKB approach is to study the upper bounds of the approximation error.[37] These bounds can be estimated for each of the intervals I, II, and III as

$$|\delta_{\pm}| \leq \exp\left[\frac{F_{\pm}(\varepsilon)}{2}\right]-1 \leq \frac{F_{\pm}(\varepsilon)/2}{1-F_{\pm}(\varepsilon)/4} , \tag{83}$$

where

$$F_{+}(\varepsilon)=\int_{\varepsilon_{\min}}^{\varepsilon} \frac{1}{p^{1/4}}\left|\frac{d^2}{d\varepsilon^2}\left[\frac{1}{p^{1/4}}\right]\right| d\varepsilon \tag{84a}$$

and

$$F_{-}(\varepsilon)=\int_{\varepsilon}^{\varepsilon_{\max}} \frac{1}{p^{1/4}}\left|\frac{d^2}{d\varepsilon^2}\left[\frac{1}{p^{1/4}}\right]\right| d\varepsilon . \tag{84b}$$

The interval $(\varepsilon_{\min},\varepsilon_{\max})$ can be infinite, provided the integrals in relationships (84) converge. A typical example of the upper bound of the WKB error is given in Fig. 29. This error should be interpreted as the maximum error for the solution of the homogeneous Boltzmann equation.

Dependence of the inelastic rate coefficients on the electron distribution

The rate coefficients for the electron-impact excitation (C_{12}) and the electron-impact ionization (S_{1c}, S_{2c}) are

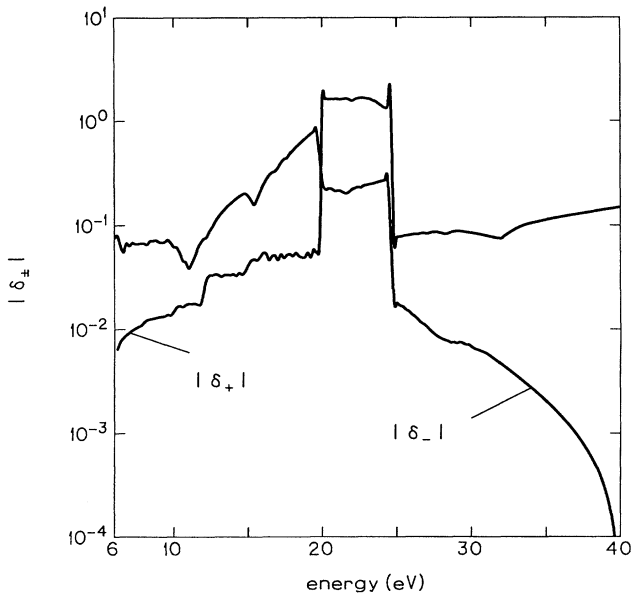

FIG. 29. The error upper bound $|\delta_{\pm}|$ for WKB homogeneous solutions f^{+} and f^{-}, respectively, for $T_e=10\,000$ K, $T_a=5000$ K, $N_1=10^{10}$ cm^{-3}, $H_{n_{\max}}=10^{-14}$, and $B_2=10^{-3}$ (case A).

TABLE I. The ratios γ in helium plasma (case A; see Fig. 10) with $T_e=10\,000$ K, $T_a=5000$ K, $N_1=10^{10}$ cm^{-3}, and $B_2=10^{-1}$.

$H_{n_{\max}}$	γ_{12}	γ_{1c}	γ_{2c}
10^{-6}	0.873	0.748	0.987
10^{-10}	4.226×10^{-2}	3.330×10^{-2}	0.599
10^{-14}	4.926×10^{-2}	3.111×10^{-2}	2.058×10^{-2}

TABLE II. The ratios γ in helium plasma (case A; see Fig. 11) with $T_e=15\,000$ K, $T_a=10\,000$ K, $H_{n_{\max}}=10^{-6}$, and $B_2=10^{-3}$.

N_1 (cm^{-3})	γ_{12}	γ_{1c}	γ_{2c}
10^{10}	1.000	1.000	0.995
10^{14}	0.916	0.760	0.991
10^{18}	2.300×10^{-2}	9.309×10^{-4}	0.701

TABLE III. The ratios γ in helium plasma (case B; see Fig. 14) with $T_e=10\,500$ K, $T_a=7000$ K, $N_1=10^{18}$ cm^{-3}, and $H_{n_{\max}}=10^{-6}$.

B_2	γ_{12}	γ_{1c}	γ_{2c}
10^{3}	5.216×10^{2}	3.782×10^{2}	0.170
10^{5}	4.984×10^{4}	3.625×10^{4}	7.948×10^{1}
10^{6}	3.559×10^{5}	2.527×10^{5}	2.959×10^{3}

TABLE IV. The ratios γ in helium plasma (case B; see Fig. 18) with $T_e=15\,000$ K, $T_a=10\,000$ K, $H_{n_{\max}}=10^{-6}$, and $B_2=10^{6}$.

N_1 (cm^{-3})	γ_{12}	γ_{1c}	γ_{2c}
10^{10}	2.592×10^{2}	5.773×10^{2}	1.060
10^{14}	1.583×10^{3}	9.328×10^{2}	6.340×10^{1}
10^{16}	1.812×10^{3}	9.399×10^{2}	7.596×10^{2}

TABLE V. The ratios L in helium plasma (case B; see Fig. 14) with $T_e=10\,500$ K, $T_a=7000$ K, $N_1=10^{18}$ cm^{-3}, and $H_{n_{\max}}=10^{-6}$.

B_2	L_{2c}	L_{AI}	L_{PI}
10^{3}	1.963×10^{2}	3.313×10^{2}	1.600×10^{4}
10^{5}	9.628×10^{4}	1.569×10^{5}	7.578×10^{6}
10^{6}	5.117×10^{6}	1.015×10^{8}	4.905×10^{9}

TABLE VI. The ratios L in helium plasma (case B; see Fig. 18) with $T_e=15\,000$ K, $T_a=10\,000$ K, $H_{n_{\max}}=10^{-6}$, and $B_2=10^6$.

N_1 (cm^{-3})	L_{2c}	L_{AI}	L_{PI}
10^{10}	7.763×10^5	2.172×10^4	1.791×10^6
10^{14}	2.879×10^7	1.306×10^7	1.077×10^9
10^{16}	3.414×10^8	5.824×10^9	4.804×10^{11}

TABLE VII. The ratios L in helium plasma (case D; see Fig. 24) with $T_e=10\,000$ K, $T_a=5000$ K, $N_1=10^{18}$ cm^{-3}.

$H_{n_{\max}}$	B_2	L_{2c}	L_{AI}	L_{PI}
1	10^4	1.039×10^3	5.509	1.606×10^2
10^3	10^4	4.915×10^3	7.218×10^{-1}	2.105×10^1
1	10^6	2.166×10^3	6.281×10^2	1.832×10^4
10^3	10^6	5.414×10^3	7.658×10^1	2.233×10^3

studied by introducing ratios of these coefficients to their values when the electron distribution is Maxwellian (C_{12}^*, S_{1c}^*, S_{2c}^*),

$$\gamma_{12}=\frac{C_{12}}{C_{12}^*},\quad \gamma_{1c}=\frac{S_{1c}}{S_{1c}^*},\quad \gamma_{2c}=\frac{S_{2c}}{S_{2c}^*}\ . \tag{85}$$

Examples of these ratios are given in Tables I–IV. As can be seen from Tables I and II, the rate coefficients for the inelastic processes, especially those with large energy gaps, are smaller in cases A than corresponding values obtained from the Maxwellian distribution. This is a result of the fact that the distribution tails are strongly underpopulated in such cases. In cases B (Tables III and IV), the ratios γ are typically much greater than one, which emphasizes the role of the strong overpopulation of the tails of the electron distributions in these plasmas.

Role of various ionization processes

We compare the electron-impact ionization of metastable atoms and the associative and Penning ionization with the electron-impact ionization of the ground-state atoms by introducing the following ratios:

$$L_{2c}=\frac{N_eN_2S_{2c}}{N_eN_1S_{1c}},\quad L_{\mathrm{AI}}=\frac{N_2N_2S_{\mathrm{AI}}}{N_eN_1S_{1c}},\quad L_{\mathrm{PI}}=\frac{N_2N_2S_{\mathrm{PI}}}{N_eN_1S_{1c}}\ . \tag{86}$$

Examples of these ratios are given in Tables V–VII. As can be seen there, there is a broad range of conditions where the production of electrons by electron-impact ionization of the ground-state atoms is negligible when compared with the associative and Penning ionization and the electron-impact ionization of the metastable atoms. Thus in such situations the form of the electron distribution above 40 eV is not important. This is of great importance for applicability of the Fokker-Planck formalism (instead of the Balescuo-Lenard formalism) to determine the electron-electron collision integrals in helium plasmas with high density of the metastable atoms. As mentioned before, in such plasmas the Fokker-Planck collision integrals may cause unrealistic, periodic humps on the high-energy (above 40 eV) tail of the electron distribution. Since these plasmas are typically in categories B and D, it is sufficient in such cases to work with the low- and medium-energy (up to about 40 eV) parts of the electron distribution based on the Fokker-Planck electron-electron integrals.

SUMMARY

A stationary electron energy distribution can exist for a meaningful period of time in the beginning of the steady-state phase following the transient phase in partially ionized helium. During this period, the densities of the electrons and the metastable atoms can be much higher than their LTE values. These densities depend on the way in which energy is supplied to the plasma in the transient phase preceding the steady-state phase. In some situations one has an unusually large, when comparing to the Maxwellian distribution, number of fast electrons (with energies of 5–30 eV) produced mainly by the associative and Penning ionization and by the electron-impact deexcitation of the metastable atoms.

In stationary plasmas where the electron and the metastable atom densities are lower than their LTE values, the tail of the electron distribution is lower than the tail of the Maxwellian distribution. Also, in such plasmas, the tail of the distribution does not have to decrease monotonically (as one tends to believe on the basis of the earlier work for gases such as argon or hydrogen) but it may have humps caused by the electron-impact deexcitation of the metastable atoms.

The Fokker-Planck collision integrals for electron-electron interactions can be used instead of the Balescu-Lenard integrals in the Boltzmann equation when the resulting distribution is to be used for calculating the rate coefficients for inelastic processes, even those with large energy gaps. Such a procedure is valid even in cases when population of the metastable atoms is much higher than its LTE value.

ACKNOWLEDGMENTS

The authors thank Rad Lyagushchenko for valuable comments. This work was supported by the National Aeronautics and Space Administration, Grant No. NAGW-1061, by the Air Force Office of Scientific Research, Grant No. 88-0119, and the University Research Initiative Grant No. 90-0170.

[1]C. G. Braun and J. A. Kunc, Phys. Fluids **30**, 499 (1987).
[2]C. G. Braun and J. A. Kunc, Phys. Fluids **31**, 671 (1988).
[3]E. C. Shoub, Astrophys. J. Suppl. Ser. **34**, 259 (1977).
[4]J. F. Shaw, M. Mitchner, and C. H. Kruger, Phys. Fluids **13**, 325 (1970).
[5]A. A. Belevstev and A. K. Mnatsakanyan, High Temp. (USSR) **13**, 943 (1975).
[6]A. B. Blagoev, Y. M. Kagan, N. B. Kolokolov, and R. I.

Lyagushchenko, Zh. Tekh. Fiz. **44**, 339 (1974) [Sov. Phys.—Tech. Phys. **79**, 215 (1974)].
[7]A. N. Soldatov and N. A. Prilezhaeva, Izv. Vyssh. Uchebn. Zaved. Fiz. **11**, 51 (1971) [Sov. Phys. J. **14**, 1500 (1971)}.
[8]A. N. Soldatov, Opt. Spektrosck. **31**, 81 (1971) [Opt. Spectrosc. (USSR) **31**, 97 (1971)].
[9]I. P. Shkarofsky, T. W. Johnston, and M. P. Bachynski, *The Particle Kinetics of Plasmas* (Addison-Wesley, London, 1966).
[10]J. R. Viegas, Ph.D. thesis, Stanford University, 1967.
[11]M. Mitchner and C. Kruger, Jr., *Partially Ionized Gases* (Wiley, New York, 1973).
[12]N. Peyraud, Phys. Fluids **21**, 1490 (1978).
[13]N. Peyraud, Phys. Fluids **20**, 2037 (1977).
[14]N. Peyraud, Phys. Fluids **18**, 1477 (1975).
[15]R. Balescu, *Statistical Mechanics of Charged Particles* (Wiley, New York, 1963).
[16]M. Hayashi, Institute of Plasma Physics, Nagoya University, Report No. 19, 1981 (unpublished), p. 21.
[17]J. Oxenius, *Kinetic Theory of Particles and Photons* (Springer-Verlag, Berlin, 1986).
[18]J. C. Ingraham and S. C. Brown, Phys. Rev. **138**, A1015 (1965).
[19]B. J. Garrison, W. H. Miller, and H. F. Schaefer, J. Chem. Phys. **59**, 3193 (1973).
[20]J. A. Kunc, Phys. Fluids **30**, 2255 (1987).
[21]H. C. Hayden and N. G. Utterback, Phys. Rev. A **135**, 1575 (1964).
[22]W. K. Peterson, E. C. Beaty, and C. B. Opal, Phys. Rev. A **5**, 712 (1972).
[23]C. B. Opal, E. C. Beaty, and W. K. Peterson, At. Data **4**, 209 (1972).
[24]T. Scott and M. R. C. McDowell, J. Phys. B **8**, 1851 (1975).
[25]R. K. Janev, W. D. Langer, K. Evans, and D. E. Post, *Elementary Processes in Hydrogen-Helium Plasmas* (Springer-Verlag, Berlin, 1987).
[26]A. W. Johnson and J. B. Gerardo, Phys. Rev. A **7**, 925 (1973).
[27]A. Dalgarno (private communication).
[28]A. B. Blagoev, Y. M. Kagan, N. B. Kolokolov, and R. I. Lyagushchenko, Zh. Tekh. Fiz. **44**, 333 (1974) [Sov. Phys.—Tech. Phys. **19**, 211 (1974)].
[29]R. I. Lyagushchenko (private communication).
[30]R. A. Demirkhanov, Yu. V. Kursanov, and L. P. Skripal, Zh. Tekh. Fiz. **44**, 1424 (1974) [Sov. Phys.—Tech. Phys. **19**, 891 (1975)].
[31]J. A. Kunc and W. H. Soon, Phys. Rev. A **40**, 5822 (1989).
[32]W. H. Soon and J. A. Kunc, Phys. Rev. A **41**, 825 (1990).
[33]W. H. Soon and J. A. Kunc, Phys. Rev. A **41**, 4531 (1990).
[34]R. I. Lyagushchenko, Zh. Tekh. Fiz. **42**, 1130 (1972) [Sov. Phys.—Tech. Phys. **17**, 901 (1972)].
[35]Y. M. Kagan and R. I. Lyagushchenko, Zh. Tekh. Fiz. **34**, 1873 (1964) [Sov. Phys.—Tech. Phys. **9**, 1445 (1965)].
[36]Y. M. Kagan and R. I. Lyagushchenko, Zh. Tekh. Fiz. **34**, 821 (1964) [Sov. Phys.—Tech. Phys. **9**, 627 (1964)].
[37]F. W. J. Olver, Proc. Cambridge Philos. Soc. **57**, 790 (1961).